Wrocław University of Science and Technology
Faculty of Electronics, Photonics and Microsystems

Field of Study: Control Engineering and Robotics

MASTER THESIS

Title of Thesis:
Comparison of sensorless and sensor methods of controlling a BLDC motor

Author:
Tomasz Lubelski

Supervisor:
Dr inż. Kamil Płachta

WROCŁAW 2024

Abstract

This thesis presents a study of sensor-based and sensorless methods for controlling brushless direct current (BLDC) motors, focusing on comparing the six-step commutation method using Hall sensors with the sensorless commutation method based on back electromotive force (BEMF) zero crossing detection.

A significant part of the study involves designing and developing a custom electronic speed controller (ESC) that integrates both control methods.

The experimental analysis compares the two methods under various conditions, evaluating performance metrics such as efficiency, rotor position accuracy, and system reliability. The findings emphasize the trade-offs between the reliability of sensored control and the cost-effectiveness of sensorless control.

In conclusion, the thesis offers insights into selecting the appropriate BLDC motor control method based on specific application needs, balancing simplicity, cost, and reliability.

Keywords: BLDC motor, control methods, sensored, sensorless, Hall sensors, BEMF, ESC, EV

Streszczenie

Niniejsza praca przedstawia badania nad metodami sterowania bezszczotkowymi silnikami prądu stałego (brushless direct current, BLDC) z wykorzystaniem czujników Halla oraz metodami bezczujnikowymi, koncentrując się na porównaniu metody komutacji sześciostopniowej z wykorzystaniem czujników Halla oraz metody bezczujnikowej opartej na wykrywaniu punktu zerowego wstecznej siły elektromotorycznej (back electromotive force, BEMF).

Znaczna część pracy obejmuje zaprojektowanie i opracowanie niestandardowego elektronicznego regulatora prędkości (electronic speed controller, ESC), który integruje obie metody sterowania.

Analiza eksperymentalna porównuje obie metody w różnych warunkach, oceniając wskaźniki wydajności takie jak efektywność, dokładność wykrywania położenia wirnika i niezawodność systemu. Wyniki podkreślają kompromisy między niezawodnością sterowania z czujnikami, a efektywnością kosztową sterowania bezczujnikowego.

Podsumowując, praca dostarcza informacji na temat wyboru odpowiedniej metody sterowania silnikami BLDC w zależności od specyficznych wymagań aplikacji, uwzględniając równowagę między prostotą, kosztami a niezawodnością.

Słowa kluczowe: silnik BLDC, metody sterowania, czujnikowe, bezczujnikowe, czujniki Hall'a, BEMF, ESC, EV

Contents

For typesetting this thesis, the LaTeX document preparation system has been used. LaTeX has been developed by L. Lamport [1], and is an overlay on top of the TeX system [2]. Mathematical fonts called AMS Euler which have been used in this document, have been commissioned by the American Mathematical Society and designed by H. Zapf [3] with the assistance of D. Knuth and his students. The URW Palladio font, used for roman text, is a clone of H. Zapf's old-style typeface called Palatino [4]. Typesetting of sans-serif monospaced text has been done using Inconsolata font, created by R. Levien [5].

[1] L. Lamport. *LaTeX: A Document Preparation System*. Addison-Wesley, 1994.

[2] D. E. Knuth. *The TeXbook*. Computers & typesetting. Addison-Wesley, 1986.

[3] D. E. Knuth and H. Zapf. *AMS Euler — a new typeface for mathematics*. Toronto: University of Toronto Press: Scholarly Publishing, 1989.

[4] *Linotype Palatino nova: A classical typeface redesigned by Hermann Zapf*. Linotype Library GmbH. 2005.

[5] R. Levien. *Inconsolata*. URL: https://levien.com/type/myfonts/inconsolata.html.

Chapter 1

Introduction

Electric motors are ubiquitous in modern society, powering everything from household appliances to industrial machinery and electric vehicles. We can differentiate between various types of electric motors based on their construction, type of supply current, and control methods. Among the many types of electric motors, Brushless Direct Current (BLDC) motors have emerged as a pivotal technology, renowned for their efficiency, reliability, and adaptability across various applications.

1.1 Overview of Electric Motors

According to literature [1], at the highest level, electric motors can be broadly categorized into Direct Current (DC) motors, Alternating Current (AC) motors, and specialized types such as BLDC motors, Synchronous motors, and Induction motors. Each category has unique attributes that make them suitable for specific uses.

DC Motors, traditionally known for their simplicity and ease of control, use brushes and mechanical commutators to reverse current flow and generate torque. However, this mechanical commutation comes with downsides, including wear and tear, which necessitates regular maintenance. The introduction of BLDC motors revolutionized the DC motor landscape by eliminating these drawbacks. BLDC motors replace mechanical commutation with electronic commutation, utilizing sensors to control the switching of current in the motor windings. This advancement results in a more durable, efficient, and maintenance-free motor, making BLDC motors ideal for applications requiring high reliability and precision, such as electric vehicles, drones, and robotics.

AC Motors, encompassing both Induction and Synchronous motors, dominate industrial and commercial applications due to their robustness and efficiency. Induction motors, in particular, are the backbone of many industrial processes, known for their simple construction and ability to operate under various load conditions without requiring direct electrical connections to the rotor. Synchronous motors, on the other hand, maintain constant speed under varying loads, making them indispensable in precision applications such as conveyor systems and power generation.

Despite the dominance of AC motors in industrial applications, the rise of BLDC motors is particularly notable in sectors where energy efficiency, compactness, and precise control are paramount. For instance, in electric vehicles, the high power density and superior torque control of BLDC motors provide the performance needed for modern, eco-friendly transportation. Similarly, in household appliances, BLDC motors contribute to quieter operation and reduced energy consumption, aligning with the growing demand for energy-efficient solutions.

The superiority of BLDC motors lies in their design and operation. As synchronous motors, BLDC motors have a rotor that moves in sync with the magnetic field generated by the stator. The absence of brushes not only reduces mechanical wear but also eliminates the sparking that can occur in brushed motors, making BLDC motors safer and more suitable for volatile environments. Additionally, the electronic control inherent in BLDC motors allows for greater precision in speed and torque control, enabling their use in applications that require fine-tuned performance, such as robotics, medical devices, and precision manufacturing.

Furthermore, the adaptability of BLDC motors extends to their ability to be customized for various voltage levels and configurations, allowing them to be used in everything from small, battery-powered devices to large industrial machines. This versatility, combined with their superior performance characteristics, positions BLDC motors as a key technology in the transition to more advanced and sustainable electric motor-driven systems.

In specialized applications, other motor types like **Switched Reluctance Motors** (SRM) and **Stepping Motors** are also employed, but even in these areas, the influence of BLDC motor technology is being felt. For example, SRMs, which are valued for their simple construction and robustness, are sometimes combined with principles from BLDC motors to enhance performance and efficiency.

Brushless Direct Current (BLDC) motors have become a pivotal technology in various modern applications due to their efficiency, reliability, and adaptability. These motors belong to the class of synchronous motors, meaning that the speed of the rotor is directly related to the frequency of the supplied current. Unlike traditional DC motors, BLDC motors do not use brushes for commutation. Instead, they rely on electronic commutation, which offers significant advantages in terms of performance, durability, and maintenance.

1.2 Historical background

The concept of a brushless motor was first introduced in the early 20th century, marking a significant departure from the traditional design of DC motors, which relied on brushes and commutators for operation. Early pioneers in motor technology recognized the potential of eliminating the mechanical commutation process, which would theoretically allow for a more efficient and reliable motor. However, the technology of the time was insufficient to realize this vision, as the necessary electronic components and control systems had not yet been developed.

It wasn't until the late 20th century, with the advent of power electronics and semiconductor technology, that BLDC motors became commercially viable. The rapid progress in these fields provided the tools needed to control the timing and switching of electrical currents within the motor, enabling the precise electronic commutation that defines BLDC motors. This technological breakthrough transformed the theoretical concept into a practical and highly efficient motor that could be used in real-world applications.

The first practical applications of BLDC motors emerged in high-performance sectors such as aerospace and industrial automation. In these fields, the advantages of BLDC motors—such as their high efficiency, precise control, and low maintenance—were particularly valuable. For instance, in aerospace applications, where reliability and performance are paramount, BLDC motors offered a significant improvement over traditional motors, with their ability to deliver consistent power under demanding conditions while minimizing the risk of mechanical failure. Similarly, in industrial automation, where precision and durability are crucial, BLDC motors enabled more sophisticated and reliable automation systems, enhancing productivity and reducing downtime.

As the technology matured and the cost of power electronics decreased, BLDC motors began to proliferate into a broader range of applications. The automotive industry, in particular, recognized the potential of BLDC motors for electric vehicles (EVs). The high torque, efficiency, and compact size of BLDC motors made them ideal for EVs, where space is limited, and energy efficiency directly impacts vehicle range and performance. Today, BLDC motors are at the heart of modern electric vehicles, powering everything from the drive motors to auxiliary systems such as power steering and cooling pumps.

In addition to the automotive sector, BLDC motors have become increasingly common in household appliances, where their quiet operation and energy efficiency offer significant benefits over traditional motors. In appliances like washing machines, refrigerators, and air conditioners, BLDC motors contribute to reduced energy consumption, lower operating costs, and quieter performance, all of which are highly desirable attributes in the consumer market.

The robotics industry has also embraced BLDC motors due to their precision and controllability. Robots often require motors that can provide fine-tuned movement with high reliability, making BLDC motors an ideal choice. From industrial robots that perform repetitive tasks with high precision to service robots in healthcare and hospitality, BLDC motors enable the advanced functionalities required in these cutting-edge technologies.

The proliferation of BLDC motors has also extended to other areas such as renewable energy systems, where they are used in wind turbines and solar panel tracking systems. Their efficiency and reliability are crucial in maximizing the energy output and ensuring long-term operation in these environmentally critical applications.

As the 21st century progresses, the development and application of BLDC motors continue to evolve. Advances in materials science, such as the use of rare-earth magnets, have further improved the performance of BLDC motors, allowing for even greater power density and efficiency. Meanwhile, ongoing innovations in control algorithms and power electronics are enabling more sophisticated and responsive motor control, opening up new possibilities for BLDC motor applications in emerging fields such as autonomous systems and smart grids.

1.3 BLDC Motors characteristics

Brushless DC (BLDC) motors offer a range of advantages that make them the preferred choice in many modern applications. These benefits stem from their unique design, which eliminates the need for brushes and relies on electronic commutation. Below are some of the key advantages that contribute to the widespread adoption of BLDC motors in various industries:

- **High Efficiency** – BLDC motors are known for their high efficiency, which is primarily due to the absence of brush friction losses. The electronic commutation system ensures that the motor operates at optimal efficiency across a wide range of speeds and loads.
- **Low Maintenance** – Without brushes to wear out, BLDC motors require significantly less maintenance than their brushed counterparts. This makes them ideal for applications where reliability and long operational life are essential.
- **Compact Size and High Power Density** – BLDC motors offer a high power-to-weight ratio, which allows for more compact and lightweight motor designs. This is particularly important in applications like drones, electric vehicles, and portable tools, where space and weight are critical considerations.
- **Precise Control** – The electronic commutation system of BLDC motors allows for precise control of motor speed and torque. This is essential in applications that require high accuracy and responsiveness, such as robotics and CNC machines.
- **Quiet Operation** – The absence of brushes not only reduces wear but also minimizes noise. BLDC motors operate more quietly than brushed motors, making them suitable for use in noise-sensitive environments, such as medical devices and home appliances.

1.4 Project Motivation

Purpose of the work

The primary purpose of this work is to conduct a comprehensive comparison between sensor-based and sensorless methods for controlling Brushless Direct Current (BLDC) motors.

Scope of the work

This thesis begins with a detailed review of the fundamental principles governing BLDC motors, establishing the necessary theoretical foundation to understand the nuances of the control methods under investigation. Following this, the work delves into the theoretical analysis of the two selected control methods: the Hall-sensor-based method and the BEMF zero-cross detection sensorless method. This analysis explores the operational mechanisms, advantages, and limitations of each approach. Subsequently, the thesis covers the design and implementation of an electronic speed controller tailored to the BLDC motor, integrating both hardware and software components necessary for executing the selected control strategies. The software development aspect of this work involves writing and optimizing control algorithms specific to both the sensor-based and sensorless methods. Finally, the scope extends to experimental research where the performance of these control methods is compared with a focus on overall reliability.

Thesis of the work

The thesis of the work is that the sensor-based BLDC motor control method provides smooth speed control over a wider range compared to the sensorless control method, what the work aims to confirm through experimental research.

Chapter 2

BLDC Motors fundamentals

This chapter provides an overview of the fundamental principles of Brushless Direct Current (BLDC) motors, focusing on their construction, operation, and control methods.

2.1 Construction and classification of BLDC motors

As depicted on Fig. 2.1 a BLDC motor consists of a stator, which is the stationary part of the motor, and a rotor, which is the rotating part. The stator is typically made up of laminated steel stacked to form a core with slots that hold the windings. These windings are energized in a sequence that generates a rotating magnetic field. The rotor, on the other hand, is fitted with permanent magnets that follow the stator's magnetic field, thus causing the rotor to turn.

Typically, BLDC motors have 3 phases, but motors with different numbers of phases are also used in specific applications. These 3 phases are usually duplicated along the stator slots to uniformly distribute the magnetic field around the rotor. They are wound in a star or delta configuration, depending on the motor's requirements, but the star configuration is more common. In star configuration, the one end of each phase is connected to a common point, while in delta configuration, the phases are connected in series. Motors can also have different numbers of pole pairs, which determine the motor's speed and torque characteristics.

Stator and rotor configurations can vary depending on the motor's application. The two most common configurations are inrunner and outrunner motors:

- **Inrunner Motors** – In this configuration, the rotor is inside the stator. This design is commonly used in applications that require high rotational speed and torque, such as electric vehicles and industrial equipment.

- **Outrunner Motors** – Here, the rotor surrounds the stator. Outrunner motors are often used in applications like model airplanes and drones because they provide higher torque at lower speeds, making them ideal for direct drive applications.

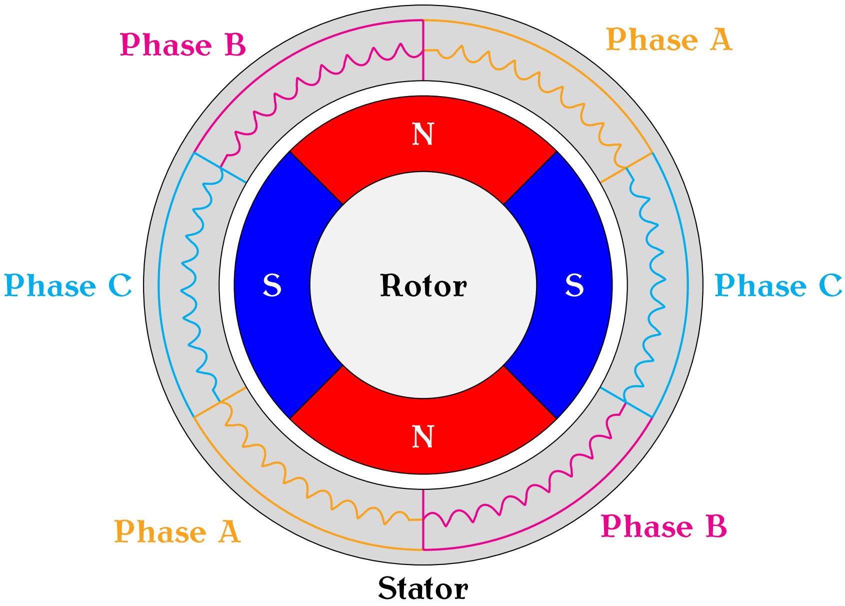

Figure 2.1 Cross-section of a six slot, two pole pair, inrunner BLDC motor

2.2 Principles of operation

2.2.1 Working principle of any electric motor

The operation of an electric motor relies on the *Lorentz force*, which is the force experienced by a current-carrying conductor in a magnetic field. This force is expressed as:

$$F = I(L \times B) \tag{2.1}$$

where:

- F is the force on the conductor,
- I is the current through the conductor,
- L is the length vector of the conductor in the magnetic field,
- B is the magnetic flux density.

This force causes the rotor in the motor to turn. In most electric motors, this interaction occurs in a loop of wire or multiple loops (windings) placed in a magnetic field generated by the stator (stationary part of the motor). The rotation is maintained by continuously reversing the current direction in the windings through a commutation process.

In an electric motor, the torque T generated is given by:

$$T = k_t \cdot I \tag{2.2}$$

where:

- T is the torque,

- k_t is the motor's torque constant,
- I is the current.

The back EMF (Electromotive Force), E_b, which opposes the applied voltage and is proportional to the motor's speed, is given by:

$$E_b = k_e \cdot \omega \tag{2.3}$$

where:

- E_b is the back EMF,
- k_e is the back EMF constant,
- ω is the angular velocity of the motor.

2.2.2 Working principle of BLDC motor

In a BLDC motor, the stator windings are energized in a sequence that creates a rotating magnetic field. The permanent magnets on the rotor align with this rotating field, producing torque.

The torque generated in a BLDC motor can be expressed as:

$$T = k_t \cdot I \cdot \sin(\theta) \tag{2.4}$$

where:

- T is the torque,
- k_t is the torque constant,
- I is the current,
- θ is the angle between the stator magnetic field and the rotor magnetic field.

Fig. 2.2 shows the idealized phase curves of currents and electromotive forces in a BLDC motor. Thy are shifted by 120° from each other. For typical BLDC motor EMF forms a trapezoidal shape, while the current is a square wave. In other motor types, like Permanent Magnet Synchronous Motors (PMSM), the EMF is sinusoidal, and the current is a sine wave. It happens due to the different rotor construction in these types of motors. It is worth noting that this distinction is not strict, and there are motors on the market that do not fit strictly into one of these categories.

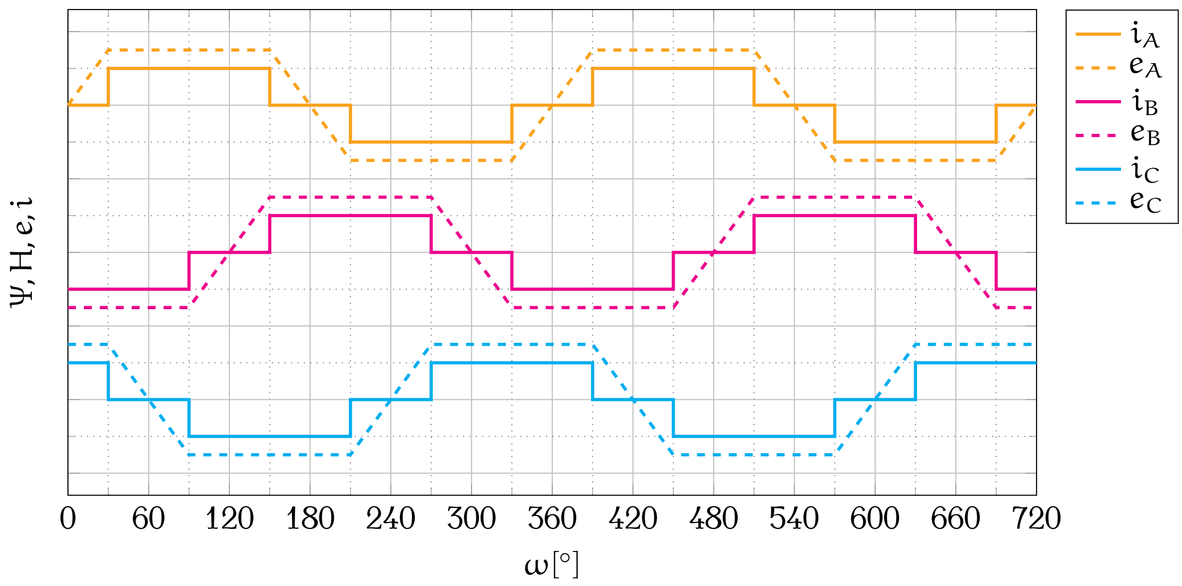

Figure 2.2 Idealized phase curves of currents and electromotive forces in a BLDC motor. Based on [2].

2.3 Electronic commutator

The most defining characteristic of a BLDC motor is its electronic commutation. Unlike brushed motors, where commutation is achieved mechanically through brushes and a commutator, BLDC motors use an electronic speed controller (ESC) to manage commutation.

This electronic commutation has several advantages:

- **Increased Efficiency:** Electronic commutation ensures that the stator's magnetic field is always optimally aligned with the rotor, which maximizes torque production and minimizes losses.
- **Flexibility in Control:** Electronic commutation allows for more sophisticated control strategies, such as Field-Oriented Control (FOC) or Direct Torque Control (DTC), which can optimize the motor's performance for specific applications.
- **Reduced Wear and Tear:** Without brushes and a mechanical commutator, there is no physical contact between moving parts that could lead to wear. This significantly extends the motor's lifespan and reduces maintenance requirements.

2.3.1 Simplified ESC implementation

Fig. 2.3 shows a simplified diagram of a BLDC motor Electronic Speed Controller (ESC). Generally the inverter consists of three half-bridge drivers that control the current flow in the motor's windings and a logic circuit that determines the switching sequence based on the rotor's position taken from sensors (e.g., Hall

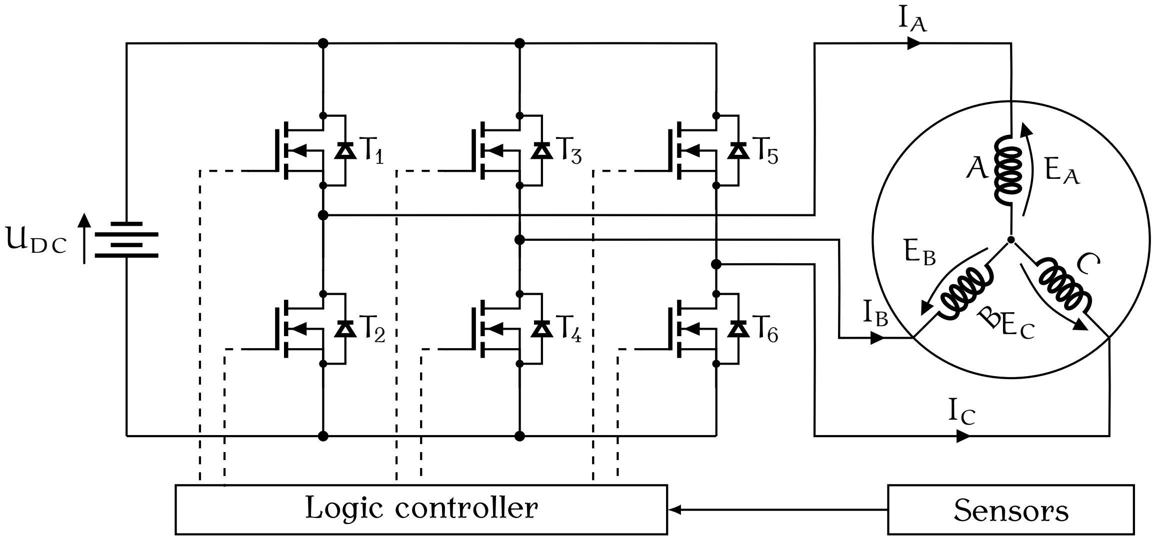

Figure 2.3 Simplified diagram of a typical BLDC motor Electronic Speed Controller. (based on [2])

effect sensors, encoders) or by measuring voltages and currents induced in the windings (sensorless methods).

Inverter switches (usually MOSFET or IGBT transistors) conduct in way that each phase can be in one of three states: positive, negative, or high impedance. Switches in one half-bridge are never opened at the same time to avoid short-circuiting the power supply. This is done by introducing a dead-time between switching the transistors.

Usually the logic circuit is implemented in a microcontroller, which also handles other tasks like communication with the master controller, parameter monitoring, and fault detection.

Chapter 3

Overview of control methods

This chapter provides an overview of the most common control methods used in BLDC motor control.

3.1 Six-step commutation

The most straightforward method of controlling a BLDC motor is six-step commutation. In this method, the motor's windings are energized in a sequence that generates a rotating magnetic field. The sequence is determined by the position of the rotor, which is detected by sensors or estimated using sensorless methods, what will be discussed in the following sections.

The six-step commutation process involves sequentially switching the current between the motor's three phases in a specific pattern that aligns with the rotor's position. Each step corresponds to a 60-degree electrical rotation of the rotor, covering the entire 360-degree cycle in six distinct steps. This method ensures that the magnetic field generated by the stator constantly pulls or pushes the rotor, maintaining continuous rotation. When a stator has three slots, so one set of coils, the electrical angle corresponds directly to the mechanical angle. However, when the stator has more slots, one mechanical revolution corresponds to multiple electrical cycles equal to the number of coil sets. Fig. 3.1 illustrates the six-step commutation sequence for a BLDC motor with six stator slots and three coil sets. We can see that with each step, the rotor moves by 30 mechanical degrees, resulting in a full 360-degree mechanical rotation after 2 full electrical cycles.

The advantages of six-step commutation include its straightforward implementation and minimal computational requirements, which make it ideal for low-cost controllers. However, the method introduces certain trade-offs, such as torque ripple and reduced smoothness in motion compared to more complex commutation methods like Field-Oriented Control (FOC). Despite its simplicity, it provides adequate performance for many BLDC motor-driven systems, especially where precision and low noise are not the primary concerns.

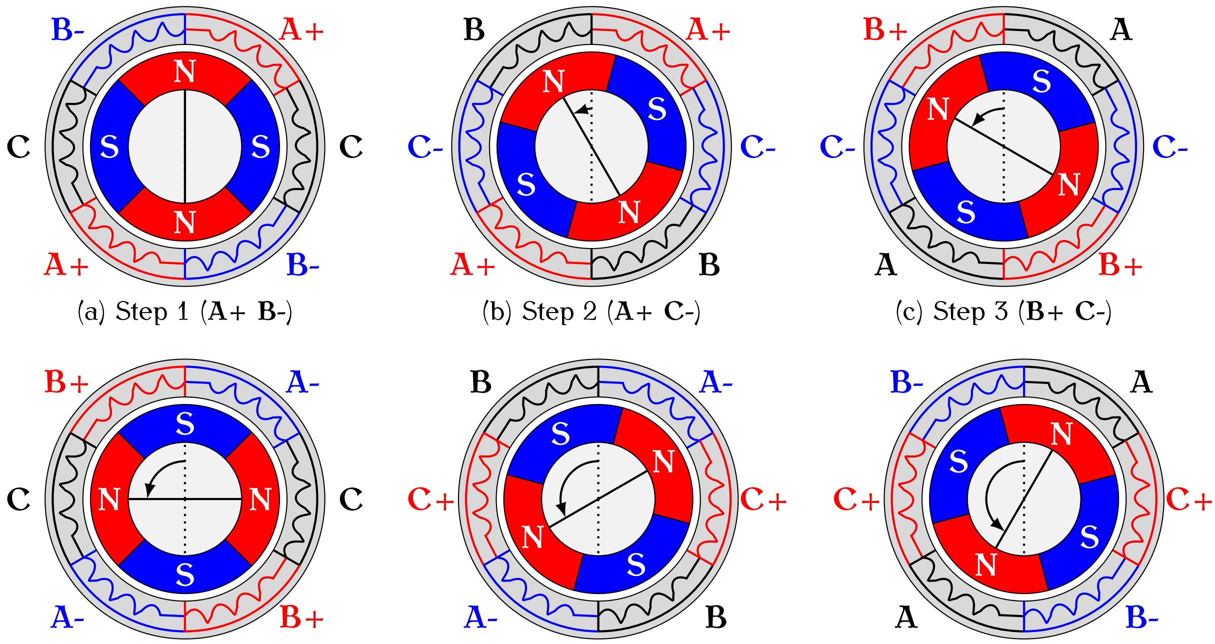

(a) Step 1 (**A**+ **B**-) (b) Step 2 (**A**+ **C**-) (c) Step 3 (**B**+ **C**-)

(d) Step 4 (**B**+ **A**-) (e) Step 5 (**C**+ **A**-) (f) Step 6 (**C**+ **B**-)

Figure 3.1 Six-step commutation sequence for one electrical cycle (based on [2])

3.2 Sensor-based position feedback

First method to determine the rotor position for the need of six-step commutation is to use sensors. This usually required the motor to be manufactured already with sensors installed or to install them manually.

For determining the BLDC motor rotor's position, we can use various types of sensors, such as:

- **Hall Effect Sensors:** These sensors are placed around the stator and detect the rotor's magnetic field by utilizing the Hall effect.
- **Absolute encoders:** These encoders provide position feedback by directly measuring the rotor's position. They can be either optical or magnetic.
- **Incremental encoders:** These encoders provide position feedback by measuring the of the rotor's position. They can be mechanical, optical or magnetic.

Hall effect sensors are the most common choice for BLDC motor control due to their simplicity and cost-effectiveness. However, they provide lower resolution than encoders and are more prone to errors due to misplacement or magnetic interference. These sensors are placed in the stator and detect the rotor's position by measuring the magnetic field generated by the rotor's permanent magnets. Depending on the motor configuration, the sensors can be placed in different positions, such as 120 degrees apart or 60 degrees apart as depicted on Fig. 3.2. Each configuration will give us a different output combinations for each step of the commutation sequence, so identification of the motor configuration is necessary to correctly interpret the sensor readings.

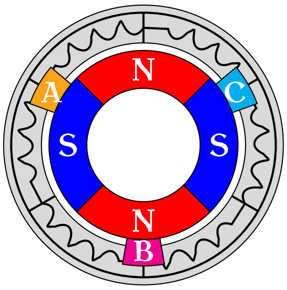

(a) 120 degrees

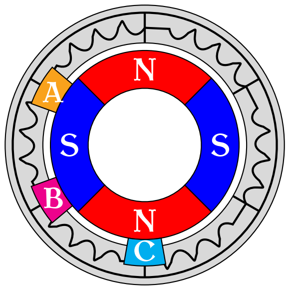

(b) 60 degrees

Figure 3.2 Possible hall sensor placement (based on [2])

Basic control models assume that the Hall sensors are placed at ideal angle from each other. Research on this topic [3] shows that misplaced sensors can lead to unbalanced conduction of the inverter switches, which can cause torque ripple and voltage spikes. To mitigate this issue, filtering and position approximation algorithms can be used.

Encoders provide high-resolution position feedback, which allows for more precise control of the motor. However, they are more expensive and usually force a specific placement on the rotor shaft, which can be challenging in some applications. Also, they incremental encoders require calibration at startup to determine the rotor's initial position. Absolute encoders require this step only once during assembly. Calibration can be done by applying voltage to two phases and waiting for the rotor to align. This gives the controller the initial position of the rotor, what is saved as a zero position.

3.2.1 Hall-effect sensor six-step commutation

Basic Hall-effect sensors output an analog voltage proportional to the strength of applied magnetic field. Sensors used in BLDC motors usually integrate additional circuitry to provide digital outputs, which are easier to process by the controller. Typically, they have open-drain outputs, which require pull-up resistors to provide a high voltage level when the sensor is not active resulting in outputting a logical `0` when the magnetic field is detected and a logical `1` when it is not. To simplify the theory of operation, we will assume that the sensors provide logical `1` when the magnetic field is detected and logical `0` when it is not.

To determine the rotor position using Hall-effect sensors, the controller should react to every change in the sensor outputs and adjust the current switches state accordingly to sequence step corresponding to the rotor position. Fig. 3.3 presents ideal phase currents and electromotive forces in conjunction with the Hall sensor outputs for a motor with 120-degree sensor placement. Achieving similar curves can be done by applying external rotation to the rotor and observing the sensors outputs. Thus, the commutation sequence can be determined empirically. Signal combinations acquired from Hall sensors with corresponding steps of the commutation sequence are presented in Table 3.2.1 for counterclockwise rotation and in Table 3.2.1 for clockwise rotation for a motor with 120-degree sensor placement.

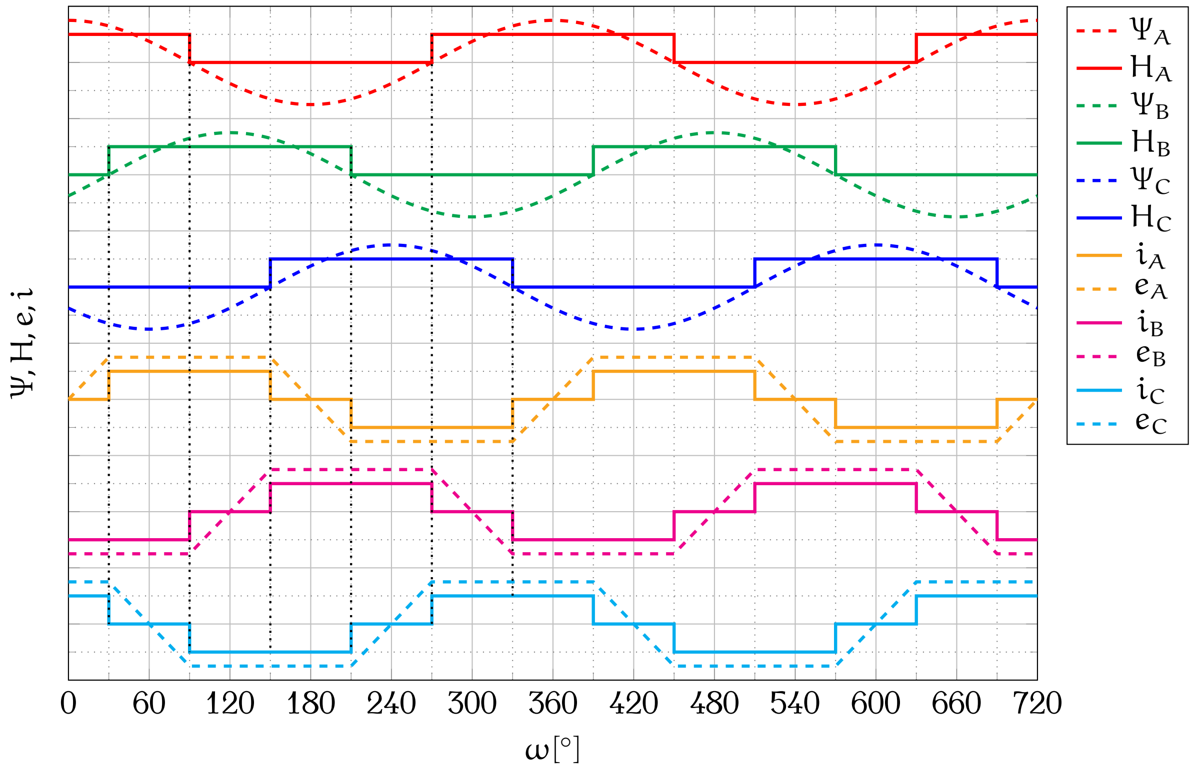

Figure 3.3 Phase fluxes with corresponding Hall sensor signals and phase electromotive forces with phase currents. Based on [2].

Table 3.1 Hall sensor states and corresponding commutation states for positive (counterclockwise) rotation (based on [2])

Step	Hall state			Phase state		
	Hall A	Hall B	Hall C	Phase A	Phase B	Phase C
1	1	1	0	+	-	0
2	0	1	0	+	0	-
3	0	1	1	0	+	-
4	0	0	1	-	+	0
5	1	0	1	-	0	+
6	1	0	0	0	-	+

Table 3.2 Hall sensor states and corresponding commutation states for negative (clockwise) rotation (based on [2])

Step	Hall state			Phase state		
	Hall A	Hall B	Hall C	Phase A	Phase B	Phase C
1	1	1	0	-	+	0
6	1	0	0	0	+	-
5	1	0	1	+	0	-
4	0	0	1	+	-	0
3	0	1	1	0	-	+
2	0	1	0	-	0	+

3.3 Sensorless position estimation

Sensorless control methods for Brushless DC (BLDC) motors are designed to eliminate the need for physical position sensors, such as Hall sensors or encoders, while still accurately controlling the motor.

One of the most common sensorless control methods is the **Back Electromotive Force (Back-EMF) Zero Crossing Detection**. This method relies on the detection of the zero-crossing point of the back-EMF, which is the voltage induced in the motor windings as the rotor spins. Since the back-EMF is directly related to the rotor position, its zero-crossing points can be used to estimate the rotor's position. In a typical BLDC motor with a trapezoidal back-EMF, during each commutation period, one phase is not powered, and the back-EMF of this phase is monitored. The zero-crossing of the back-EMF indicates that the rotor is at a specific position relative to the stator, triggering the next commutation. This method is simple and widely used, but its performance is degraded at low speeds where the back-EMF is weak, and noise can affect accuracy.

Another advanced method is the **Extended Kalman Filter (EKF)**[4], an estimation technique that predicts the motor's state, such as rotor position and speed, by processing noisy measurements of currents and voltages. The EKF uses a mathematical model of the motor and updates the estimates as new measurements are taken. The Kalman filter continuously updates its internal model of the motor's behavior based on the observed voltages and currents, providing an estimate of the rotor's position and speed. While this method offers high accuracy and robustness to noise, it is computationally intensive, requiring significant processing power.

The **Sliding Mode Observer (SMO)**[5] is based on sliding mode control theory, where the rotor position is estimated by driving the error between the actual and estimated currents to zero using a discontinuous control signal. The SMO estimates the back-EMF by observing the difference between the actual and estimated stator currents, and the rotor position is then inferred from the estimated back-EMF. This method is robust against parameter variations and disturbances, although the switching nature of the observer can introduce chattering, which may require smoothing or filtering.

Phase-Locked Loop (PLL)[6] is another method where a PLL system locks onto the phase of the back-EMF signal and tracks the rotor position by adjusting the frequency and phase of the control signal. The PLL synchronizes with the phase of the back-EMF, ensuring that the drive signals are correctly aligned with the rotor's position. This method is especially useful in applications requiring precise speed control, particularly at high speeds. However, it involves complex implementation and potential stability issues if not carefully designed.

Third Harmonic Voltage Integration[7] is another sensorless method that extracts the third harmonic component of the back-EMF, which is naturally present in a three-phase BLDC motor. The rotor position can be estimated by integrating this third harmonic signal over time. The third harmonic component is isolated from the combined phase voltages, and this signal is integrated to estimate the rotor's position. This method provides good performance across a wide range of speeds but requires precise filtering to accurately extract the third harmonic.

3.3.1 Back-EMF zero crossing six-step commutation

Fig. 3.4 illustrates the phase currents (i_A, i_B, i_C,) and the corresponding back electromotive forces (e_A, e_B, e_C,) in a BLDC motor over one electrical cycle (360°). The key features to note here are the points of zero-crossing in the back-EMF signals and the time delay τ from the zero-crossing to the commutation event. Each phase (A, B, C) generates a trapezoidal back-EMF, which alternates between positive and negative values as the rotor spins. The points at which the back-EMF of a phase crosses zero (referred to as zero crossings) are critical because they signal that the rotor's magnetic field has passed the magnetic axis of the stator phase. These zero-crossing points are used to time the commutation of the phases.

In a typical six-step commutation sequence, each step is triggered when the back-EMF of one of the unenergized phases crosses zero. However, instead of commutating immediately at the zero-crossing point, there is a deliberate time delay, denoted as τ. This delay ensures that the commutation occurs when the rotor has moved 30° past the zero-crossing point, which is the optimal position for maximizing torque production. The correct timing of this commutation is essential to align the rotor's magnetic field with the stator's magnetic field, ensuring smooth and efficient motor operation.

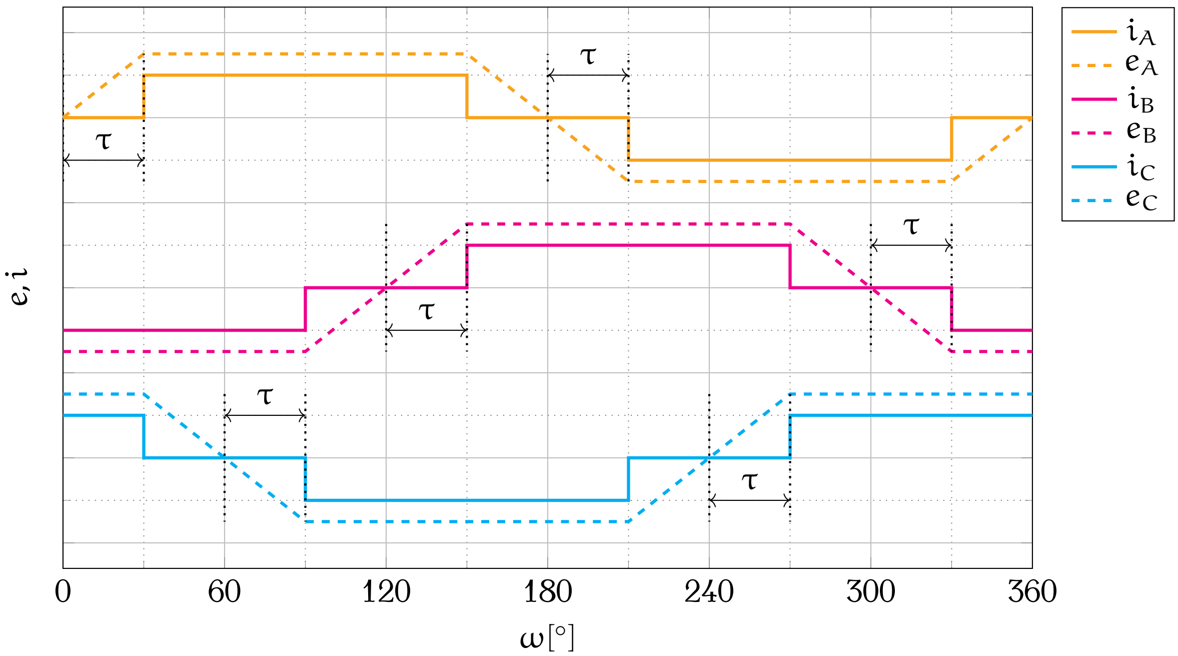

Figure 3.4 Phase electromotive forces with phase currents. Based on [2].

From the back-EMF zero-crossing points and shape of the back-EMF signals, we can derive the rising and falling edge of the back-EMF signals for each commutation step. These maps are presented in Tab. 3.3.1 for positive (counterclockwise) rotation and in Tab. 3.3.1 for negative (clockwise) rotation.

We can observe that when the Back-EMF of the unenergized phase is rising (positive slope), this phase should be energized positively. On the other hand, when the Back-EMF of the unenergized phase is falling (negative slope), this phase should be energized negatively. From these rules, we can derive that to reverse the rotation

Table 3.3 Detected BEMF edge and corresponding commutation states for positive (counterclockwise) rotation (based on [2])

Step	BEMF edge	Phase state		
		Phase A	Phase B	Phase C
1	A ↗	+	-	0
2	C ↘	+	0	-
3	B ↗	0	+	-
4	A ↘	-	+	0
5	C ↗	-	0	+
6	B ↘	0	-	+

Table 3.4 Detected BEMF edge and corresponding commutation states for negative (clockwise) rotation (based on [2])

Step	BEMF edge	Phase state		
		Phase A	Phase B	Phase C
1	A ↗	+	0	-
6	B ↘	+	-	0
5	C ↗	0	-	+
4	A ↘	-	0	+
3	B ↗	-	+	0
2	C ↘	0	+	-

direction, we need to swap polarity of the previously energized phases like in sensor-based commutation.

3.4 Speed estimation

For sensored and sensorless control methods, the speed of the motor can be estimated from average time between commutation events $t_{COMM}[s]$. For sensored method t_{COMM} is the time between changes in Hall sensor states, while for sensorless methods t_{COMM} is equal to the time between zero crossing of the back-EMF and commutation event multiplied by 2 (since the time from zero-crossing to commutation event is equal to 30°). From commutation interval we can calculate the electrical frequency of the motor:

$$f_{ELEC} = \frac{1}{t_{COMM} \cdot 6}[Hz] \tag{3.1}$$

where 6 is the number of commutation steps per electrical cycle.

The electrical frequency can be converted to the mechanical speed of the motor by dividing it by the number of pole pairs:

$$\omega = \frac{f_{ELEC}}{p}[Hz] = \frac{f_{ELEC}}{p} \cdot 60[RPM] \tag{3.2}$$

where p is the number of pole pairs.

Chapter 4

Design of an Electronic Speed Controller

This chapter describes the design of an electronic speed controller (ESC) for a brushless DC motor. It includes project requirements, selection of components, schematic design, PCB layout and final evaluation of the designed ESC.

4.1 Project requirements

Designing an electronic speed controller (ESC) for a brushless DC motor requires a set of requirements to be met. The ESC should be able to control the speed of the motor, provide feedback to the controller, and communicate with other devices in the system. The following requirements have been set:

- Compatibility with regular three-phase brushless DC motors in star configuration without center tap.
- Maximum operating voltage of 100V.
- Maximum continuous phase current of 40A.
- Maximum peak phase current of 100A.
- Possibility of using Hall-effect sensors and incremental encoders for rotor position detection.
- Measuring equipment needed for current and voltage sensing for the sake of sensorless operation.
- Ability to connect external sensors via I2C or SPI.
- Communication with the main controller via CAN bus.
- Possibility of firmware update via USB.
- No need for external cooling.

4.2 Subsystem design

The ESC consists of several subsystems that are responsible for different tasks. These subsystems power supply, power stage, microcontroller, sensors and communication. Fig. 4.1 shows the block diagram of the designed ESC. The power supply subsystem is responsible for providing power to the ESC and the motor. The power stage subsystem is responsible for switching the power to the motor windings. The sensor subsystem is responsible for measuring the current, voltage and rotor position. The microcontroller subsystem is responsible for controlling the power stage gathering data from sensors and communicating with other devices.

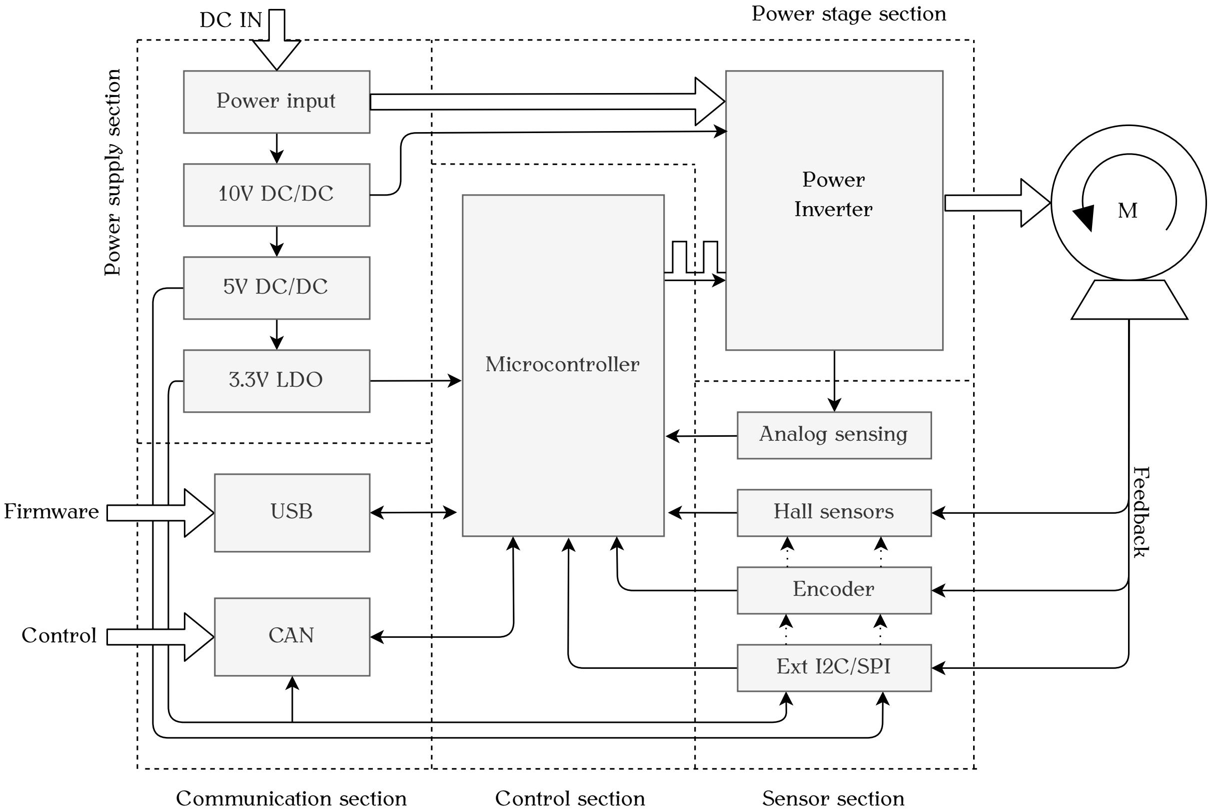

Figure 4.1 Block diagram of the designed ESC

4.2.1 Power supply subsystem

Power supply has been divided into three stages: 10V step-down converter, 5V step-down converter and 3.3V linear regulator. The 10V step-down converter provides power to mosfet gate drivers and analog circuits. The 5V step-down converter provides power to digital sensors. The 3.3V linear regulator provides power to the microcontroller and communication subsystems.

10V Step-down converter

First stage of power supply is DC-DC step-down converter in buck topology. It is designed around LM5161PWP [8] integrated circuit according to datasheet reference application. Fig. 4.2 shows the schematic of the converter. The converter is capable of delivering 1A of current at 10V output voltage. It is possible to operate at input voltage reaching 100V with low losses, because of the self-feed capability. When the output voltage stabilizes, the IC turns off the internal linear regulator and powers itself from the output voltage through the diode D2 and capacitor C13. It also features under-voltage lockout, thermal shutdown and over-current protection.

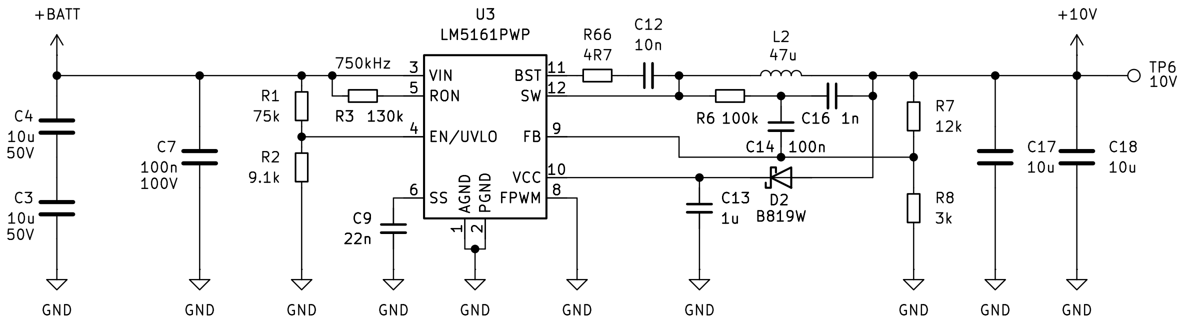

Figure 4.2 Schematic of 10V step-down converter

Output voltage has been set to 10V by selecting the appropriate resistor divider to feedback pin of the IC. It was calculated using the following formula:

$$V_{OUT} = \frac{V_{REF} \times (R_{FB2} + R_{FB2})}{R_{FB1}} \tag{4.1}$$

where $V_{REF} = 2V$. The values of resistors R_{FB2} and R_{FB1} have been calculated to be 12kΩ and 3kΩ respectively, what gives precisely 10V output voltage, without taking into account the tolerance of the resistors.

Switching frequency of the converter has been set to 750kHz by selecting the R_{ON} resistor to 130kΩ according to formula:

$$f_{SW} = \frac{V_{OUT}}{1.008 \times 10^{-10} \times R_{ON}} \tag{4.2}$$

Rest of components values have been selected according to the datasheet recommendations.

5V Step-down converter

Second stage of power supply is also a DC-DC step-down converter in buck topology. It is designed around TPS5430DDA [9] integrated circuit according to datasheet reference application. Fig. 4.3 shows the schematic of the converter. The converter is capable of delivering 2A of current at 5V output voltage. It features under-voltage lockout, thermal shutdown and over-current protection.

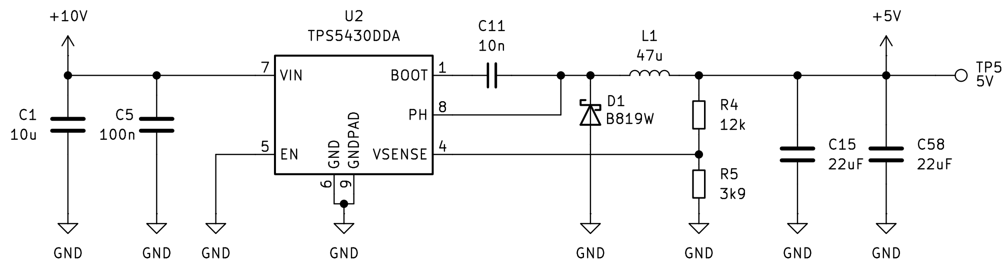

Figure 4.3 Schematic of 5V step-down converter

This converter has fixed switching frequency of 500kHz. Output voltage has been set to 5V by selecting the appropriate resistor divider to feedback pin of the IC. It was calculated using the following formula:

$$V_{OUT} = \frac{V_{REF} \times (R_{FB2} + R_{FB2})}{R_{FB1}} \tag{4.3}$$

where $V_{REF} = 1.221V$. The values of resistors R_{FB2} and R_{FB1} have been calculated to be 12kΩ and 3.9kΩ respectively, what gives approximately ≈ 4.98V output voltage, what is acceptable for the application.

Rest of components values have been selected according to the datasheet recommendations.

3.3V linear regulator

The last stage of power supply is a low-dropout linear regulator AMS1117 [10]. It provides 3.3V output voltage with maximum current of 1A. Fig. 4.2.1 shows the schematic of the regulator. It features thermal shutdown and over-current protection. It's output voltage is fixed and does not require any additional components to

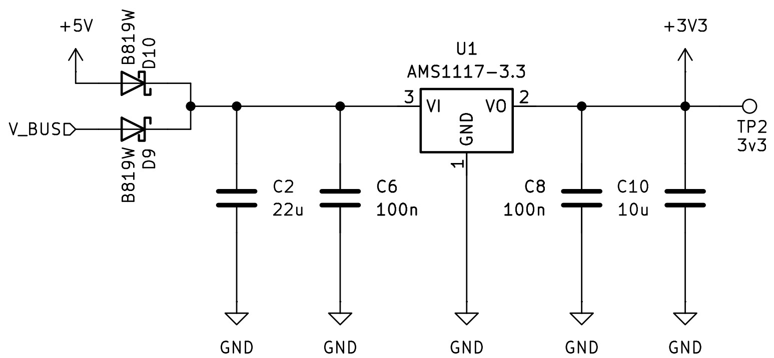

Figure 4.4 Schematic of 3.3V linear regulator

set it. The input voltage to the regulator is connected to the 5V step-down converter output, but also to USB V-BUS voltage through the diode D10 and D9 respectively. This allows to power the microcontroller from the USB port when the ESC is connected to the PC, without the need to power the whole system.

4.2.2 Power stage subsystem

Power stage subsystem is responsible for switching the power to the motor windings. It consists of three half-bridge circuits, each of them driven by common integrated smart gate driver DRV8353 [11]. Transistors used in the power stage are N-channel MOSFETs IPT015N [12]. They were selected because of their low drain-source ON resistance R_{DSON} = 1.5mA and high continuous current capability I_D = 300A and maximum drain-source voltage V_{DS} = 100V. Fig. 4.5 shows the schematic of the triple half-bridge circuit with one driver divided into three symbols for better clarity.

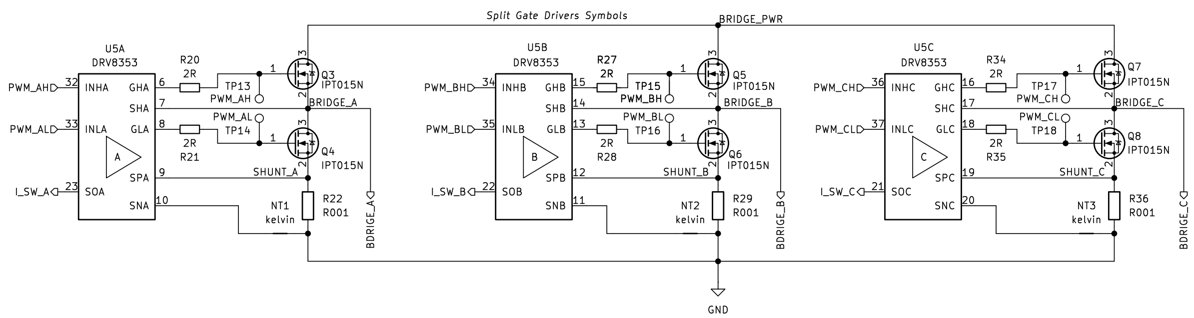

Figure 4.5 Schematic of power stage

Both high-side and low-side transistors are N-channel MOSFETs. Used smart gate driver features integrated charge pump instead of traditional bootstrap circuit. This allows to generate gate voltage higher than the supply voltage, what is required to drive high-side transistors by creating floating voltage on VCP capacitor. It also has advantage of allowing 100% duty cycle operation. The driver features over-current protection, under-voltage lockout and thermal shutdown. Problem of shoot-through current has been solved by driver's integrated dead-time generator, which ensures that high-side and low-side MOSFET in the same half-bridge are never turned on at the same time.

Dynamic brake circuit

Due to the inductive nature of the motor, it generates back electromotive force (EMF) when the power is disconnected. This energy can be used to recharge the battery, but when the battery is fully charged or the motor is powered from a power supply, it can cause overvoltage and damage the ESC and other components. To prevent this, a dynamic brake circuit has been designed. It consists of two additional transistors and an external power resistor. As shown in Fig. 4.6, when voltage on `BRIDGE_PWR` line exceeds the threshold set by the microcontroller, transistors Q1 is turned off and transistor Q2 is turned on. This shorts the motor windings and dissipates the energy in the power resistor. This additional pair of transistors is driven by separate driver IC IR2108 [13].

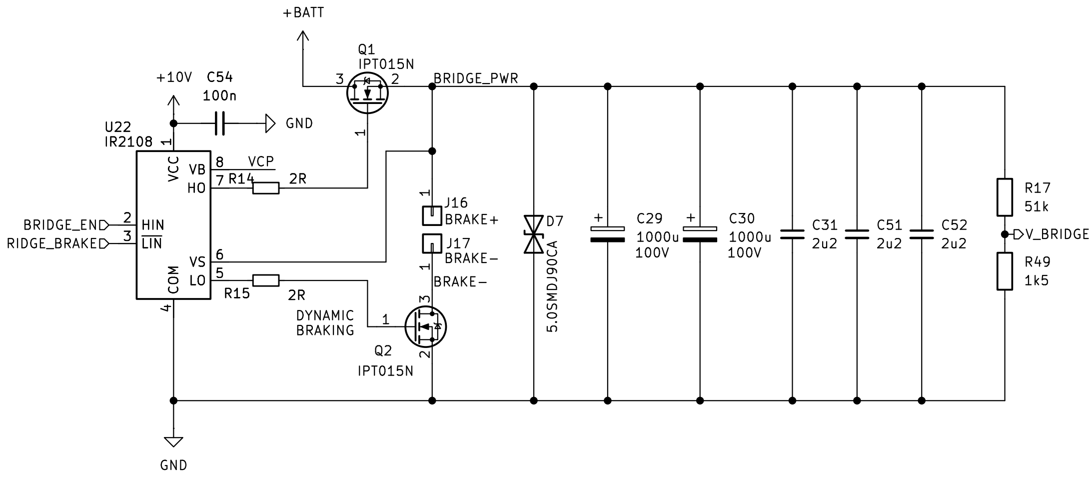

Figure 4.6 Schematic of dynamic brake circuit

4.2.3 Sensor subsystem

Sensor subsystem is responsible for measuring electrical quantities and reading the rotor position. It consists of two parts: onboard analog sensors on the power stage and external sensors connected to the board.

Internal analog sensors

For the needs of sensorless control methods the ESC is equipped with two analog measurement circuits. The first one is responsible for measuring the current flowing through the motor windings. It is based on ACS7298 [14] bidirectional Hall-effect based current sensor. The second one is responsible for measuring the back electromotive force generated by the motor. For correct position estimation phase voltages must be measured with respect to virtual neutral point created from star shaped voltage divider from each phase. This is achieved by INA149 [15] high common-mode voltage unity-gain difference amplifier. Fig. 4.7 shows the schematic of both circuits.

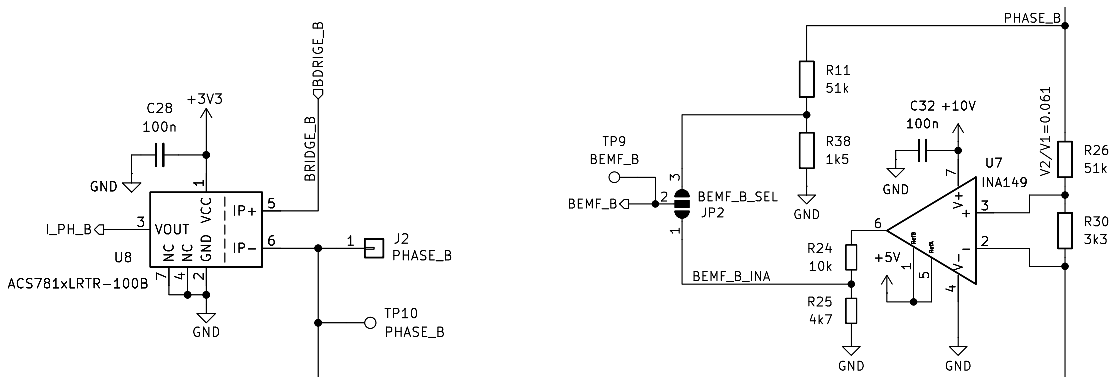

(a) Current sensing (b) BEMF sensing

Figure 4.7 Schematic of analog sensors

External sensors interface

For the needs of sensor-based control methods the ESC is equipped with interfaces for several external sensors like quadrature encoders, Hall-effect sensors or any external SPI or I2C sensors like absolute encoders. As shown in Fig. 4.8 Hall-effect sensors and incremental encoder interfaces feature 10kΩ pull-up resistors to ensure proper signal levels for microcontroller and simple low-pass filters to reduce noise. Both interfaces are protected against overvoltage by TVS diodes according to ADC input protection guidelines from the microcontroller's application note [16]

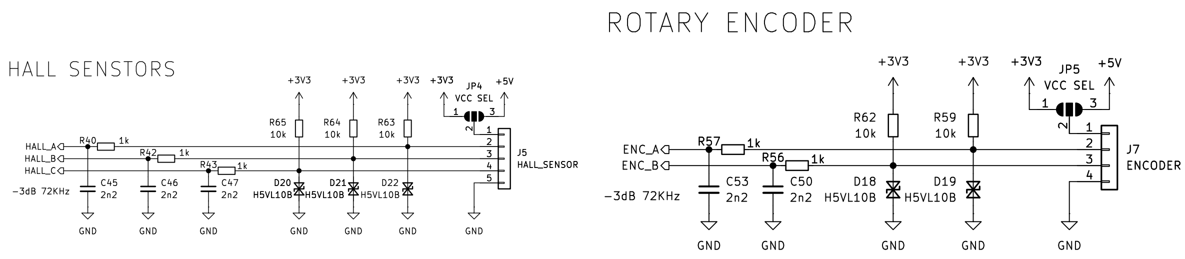

(a) Hall-effect sensors interface

(b) Encoder interface

Figure 4.8 Schematic of external sensors interfaces

4.2.4 Communication subsystem

To provide communication with the main controller or computer the ESC is equipped with two communication interfaces: USB and CAN. USB interface is used for firmware update and debugging purposes. CAN interface is used for real-time communication with the main controller. Fig. 4.9 shows the schematic of both interfaces. CAN interface is based on SN65HVD230 [17] high-speed transceiver. USB physical layer is integrated into the microcontroller. Both interfaces are protected against overvoltage by TVS diodes. CAN interface also features jumper with termination resistor $R_{TERM} = 120\Omega$ what corresponds to the impedance of the CAN bus differential line.

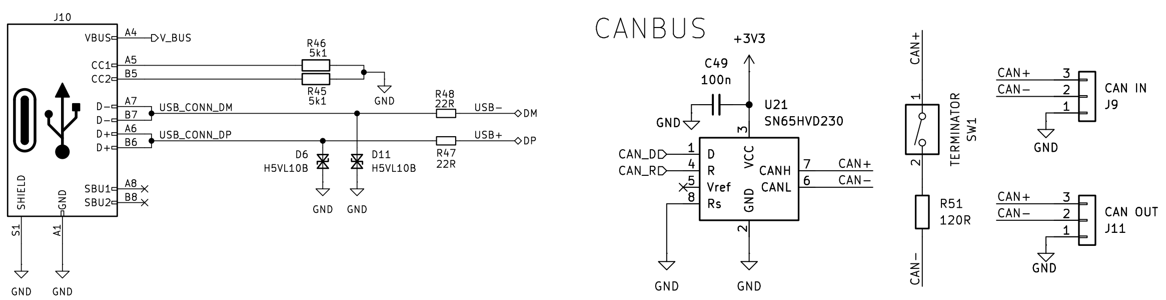

(a) USB communication

(b) CAN communication

Figure 4.9 Schematic of communication interfaces

4.2.5 Control subsystem

The heart of the ESC is the microcontroller that is responsible for controlling the power stage, gathering data from sensors and communicating with other devices. The microcontroller used in the design is STM32G474RCT6 [18]. It features ARM Cortex-M4 core with hardware floating point unit (FPU), 256kB of flash memory and 256kB of static RAM, five 12-bit analog-to-digital converters, two CANFD interfaces, and special timers designed specially for motor control like HRTIM (High-Resolution Timer). Fig. 4.10 shows the schematic of microcontroller connections.

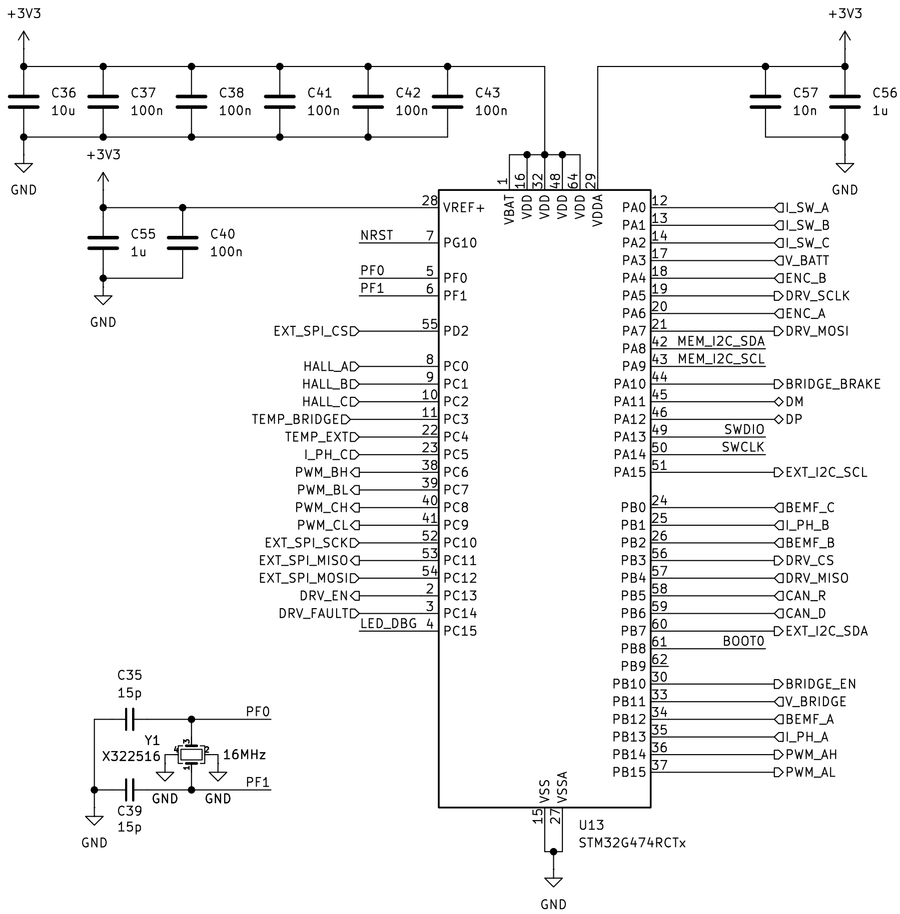

Figure 4.10 Schematic of microcontroller connections

The microcontroller is powered from the 3.3V linear regulator. Basic clock signal is generated by external 16MHz crystal oscillator, which is then internally multiplied by PLL to achieve 170MHz system clock.

Because the microcontroller does not have any internal non-volatile memory, the EEPROM memory has been added to the board. It is connected to the microcontroller via I2C bus.

4.3 Printed circuit board design

For the purpose of the project, a printed circuit board (PCB) has been designed. To provide good signal integrity, the board has been designed with controlled impedance traces as a six-layer stack-up shown in Table 4.1.

Table 4.1 PCB stack-up

Layer	Material	Thickness	Designation
Top layer	Copper	35μm	Signals and ground
Prepreg	3313*1	99.4μm	–
Inner layer 1	Copper	15.2μm	Ground plane
Core	Core	0.55mm	–
Inner layer 2	Copper	15.2μm	Signals
Prepreg	2116*1	99.4μm	–
Inner layer 3	Copper	15.2μm	Ground plane
Core	Core	0.55mm	–
Inner layer 4	Copper	15.2μm	Ground plane
Prepreg	3313*1	99.4μm	–
Bottom layer	Copper	35μm	Signals and ground

To withstand required high current traces carrying them has been designed with width of 10mm and has been repeated on all layers and connected together with vias, which has been filled and covered with copper to provide low resistance. This configuration provides capability of carrying up to 40A of continuous current with temperature rise below 20°C. Fig. 4.3 and 4.3 show the assembled PCB of the designed ESC. We can see that power traces has also exposed copper area to provide better heat dissipation and add possibility of covering them with solder to increase current carrying capability. All connections has been gold plated to provide better contact resistance and prevent oxidation.

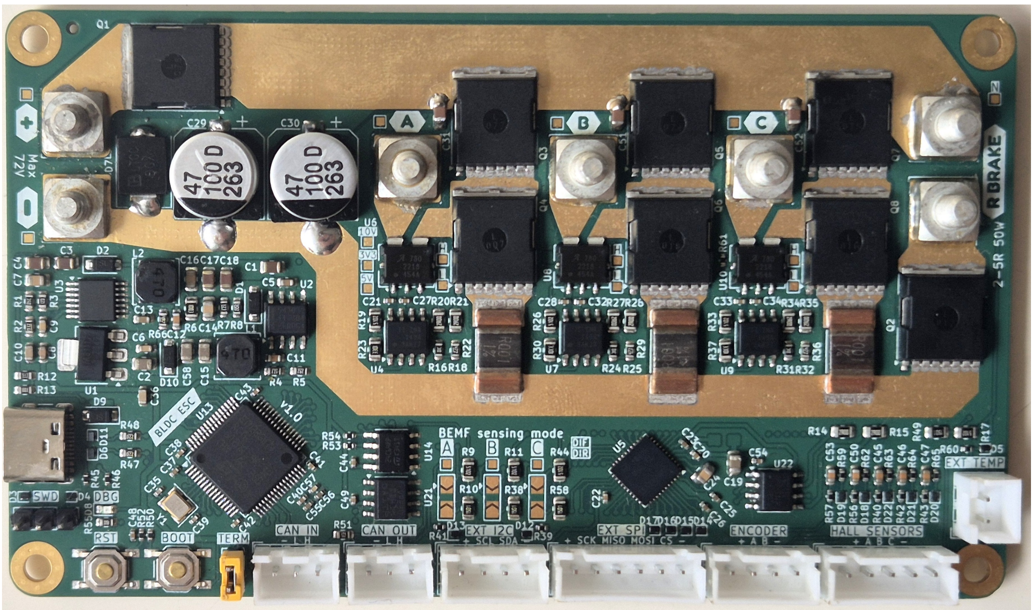

Figure 4.11 Assembled PCB of the designed ESC – top side

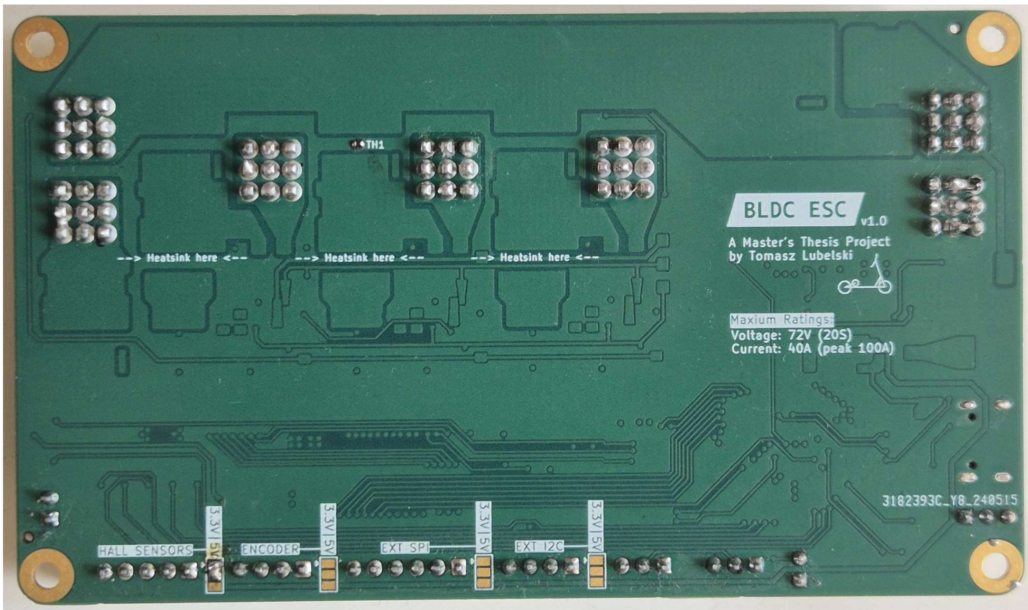

Figure 4.12 Assembled PCB of the designed ESC – bottom side

4.4 Project evaluation

To proceed with further steps, the designed ESC has been evaluated to check if it meets the requirements and functions as expected. The evaluation procedure covers the following areas:

- digital circuits functionality,
- power supply voltages and noise,
- gate driver voltages.

Evaluation of digital circuits functionality has been performed by flashing the microcontroller with a simple test firmware that toggles the GPIO pins and generates PWM signals on the motor control pins. These tests succeeded, and the microcontroller was able to control the power stage as expected what allows proceeding with detailed analysis of the voltages.

4.4.1 Supply voltages analysis

Power supply evaluation has been performed by measuring the output voltages of the 10V and 5V step-down converters and the 3.3V linear regulator. Key parameter checked was the peak-to-peak voltage ripple. The acceptable value of the ripple was set to 100mV. The measurements were performed using a digital oscilloscope in AC coupling mode and 20mV per division scale.

10V Step-down converter

Fig. 4.13 shows the scope capture of the 10V step-down converter output voltage. The peak-to-peak voltage ripple is $V_{10PP} \approx 80mV$ what is acceptable value and won't affect the operation of the gate drivers.

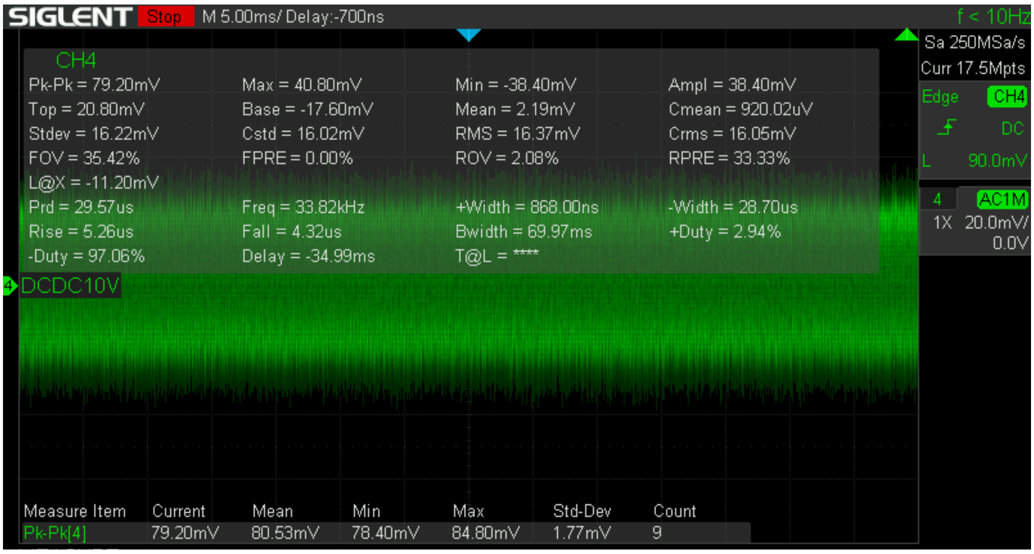

Figure 4.13 Scope capture of the voltage generated by the 10V step-down converter

5V Step-down converter

Fig. 4.14 shows the scope capture of the 5V step-down converter output voltage. The peak-to-peak voltage ripple is also $V_{5PP} \approx 80mV$ what is acceptable value and won't affect the operation of the sensors.

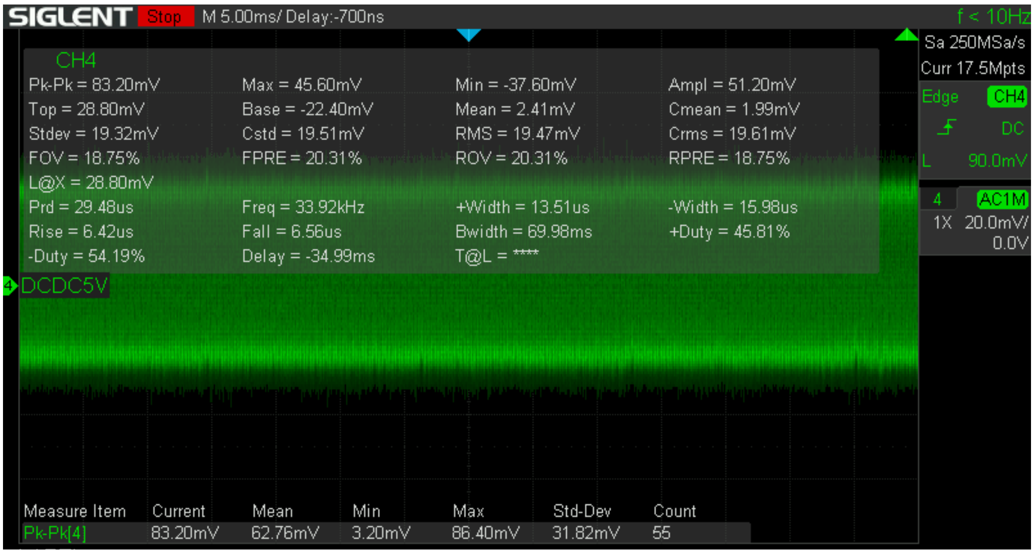

Figure 4.14 Scope capture of the voltage generated by the 5V step-down converter

3.3V linear regulator

Fig. 4.14 shows the scope capture of the 3.3V linear regulator output voltage. The peak-to-peak voltage ripple is $V_{3PP} \approx 40mV$ what is a satisfactory value especially for the microcontroller analog to digital converters.

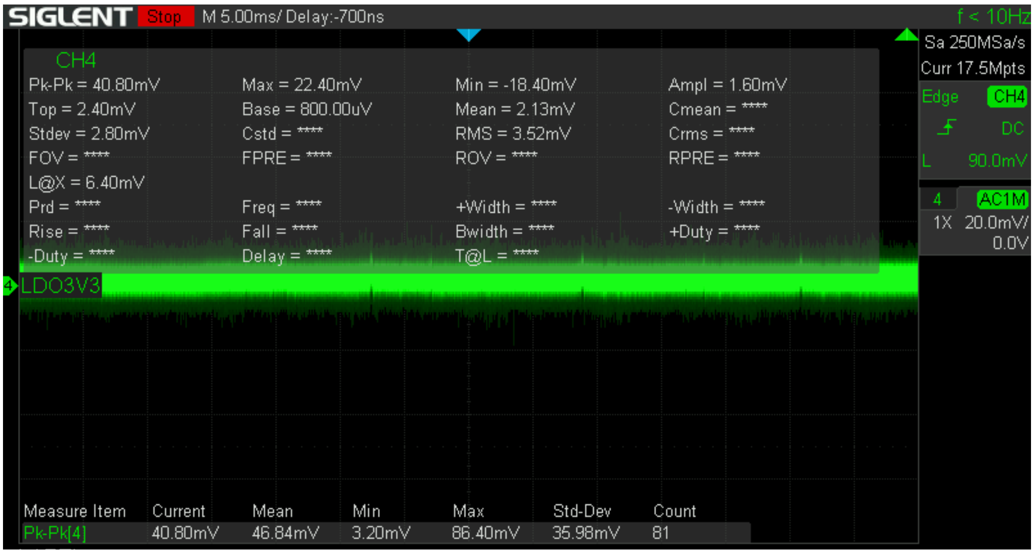

Figure 4.15 Scope capture of the voltage generated by the 3.3V linear regulator

4.4.2 Gate driver voltages analysis

Gate driver evaluation has been performed by measuring the output voltages of charge pump voltage V_{CP} during operation. The key parameter checked was the voltage level and the rise and fall times. The measurements were performed using a digital oscilloscope in AC coupling mode and 200mV per division scale. Fig. 4.16 shows the scope capture of the V_{CP} voltage.

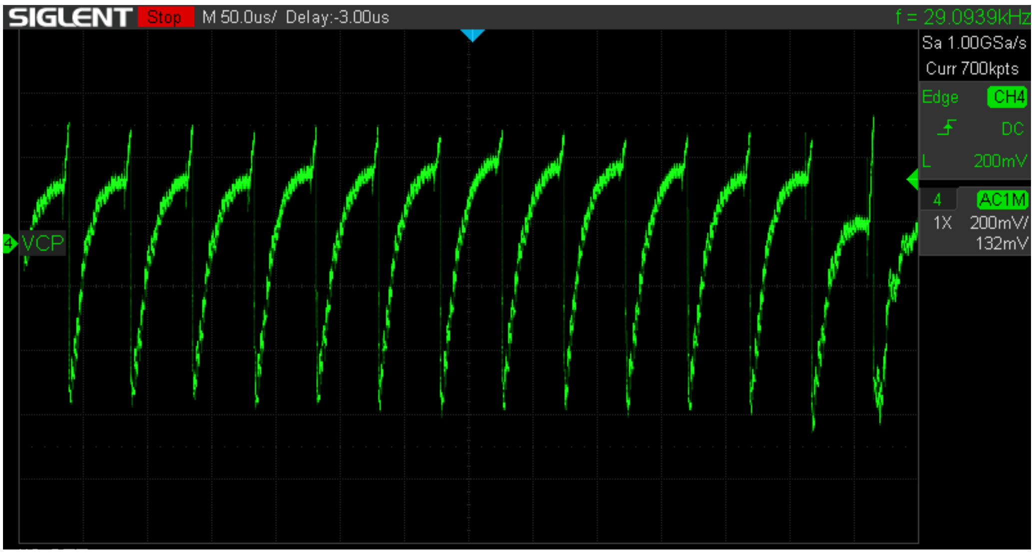

Figure 4.16 Scope capture of the V_{CP} voltage generated by the gate driver

The voltage level is 10.5V above the supply voltage, what is required to drive the high-side transistors. We can observe the cycle of charging and discharging the V_{CP} capacitor within $V_{CPPP} \approx 600mV$ peak-to-peak voltage ripple. The rise time of the voltage is $t_R \approx 50us$ what is compliant with set PWM frequency of 20kHz. The 600mV voltage drops creating minimum $V_{GS} = 10.1V$ for the high-side MOSFETs are still largly above the V_{GSth} threshold voltage what does not cause any additional switching losses.

4.5 Summary

After the evaluation, it can be concluded that the designed ESC meets the requirements and functions as expected. The power supply voltages are stable and have low ripple. The gate driver generates the required voltage levels and has fast rise and fall times. The sensor interfaces are working correctly and the digital circuits are functioning as expected. The designed ESC is ready for conducing the planned research.

Chapter 5

Software Implementation

This chapter describes the software implementation of the project including the microcontroller configuration, the peripherals used, and software strategies for implementation of selected control algorithms.

5.1 Software overview

Microcontroller selected for this project is STM32G474RCT6 [18] from STMicroelectronics in LQFP64 surface mount package. G4 [19] is a series of microcontrollers based on ARM Cortex-M4 [20] core with FPU and DSP instructions and is designated for high performance power electronics applications. It features powerful peripherals like HRTIM which is used for high resolution and high frequency PWM generation and CORDIC accelerator for fast trigonometric calculations.

The microcontroller is programmed in `C/C++` languages using STM32 HAL (Hardware Abstraction Layer) library which provides a high level API for the peripherals. For the real-time scheduling a Real Time Operating System (RTOS) is used which is FreeRTOS [21]. It allows creating multiple concurrent tasks with different priorities and provides synchronization mechanisms like semaphores and queues for inter-task communication. These mechanisms give the ability to separate the control algorithms from the hardware handling and communication tasks. For example, if some driver is busy with communication, the control algorithm can still run and update the control signals without any delay. Additionally, to provide high level data containers without using dynamic memory allocation, the Embedded Template Library (ETL) [22] is used. It is a set of `C++` templates for embedded systems which provides containers like vectors, queues, and maps with fixed allocation.

5.2 Microcontroller configuration

The microcontroller is configured using STM32CubeMX [23] software which is a graphical tool for configuring the microcontroller peripherals and generating the initialization code. Firstly the clock sources has to be configured. This project uses an external crystal oscillator with a frequency of 16MHz. According to the datasheet [18] the maximum frequency of the microcontroller is 170MHz so the PLL is configured to divide the input frequency by 4, then multiply it by 85 and finally divide it by 2 to achieve the `SYSCLK` frequency of 170MHz. The `HCLK`, `PCLK1` and `PCLK2` are set to the same frequency as `SYSCLK`. Fig. 5.1 shows the pin configuration of the microcontroller.

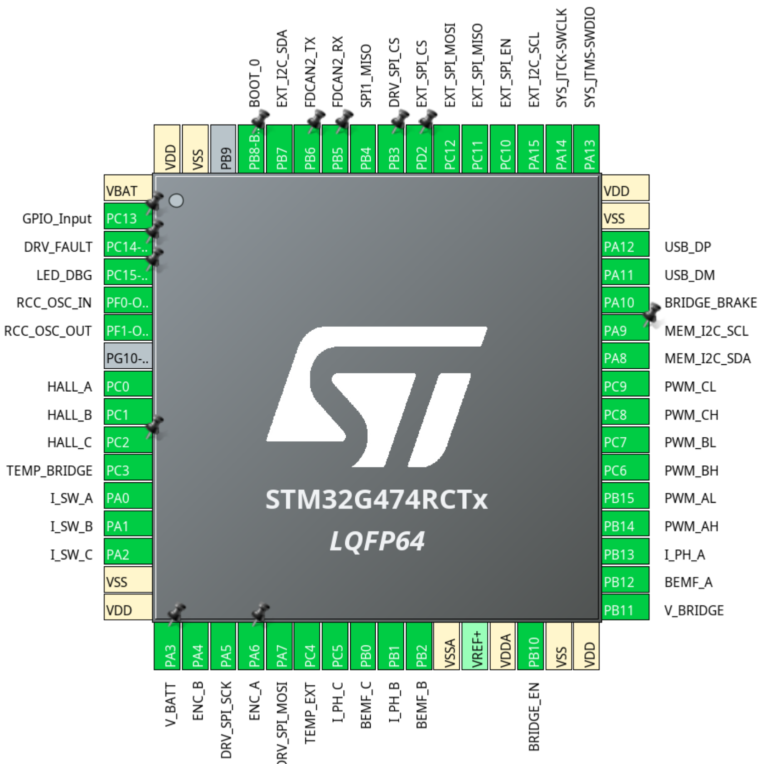

Figure 5.1 STM32G4 configuration using STM32CubeMX

5.2.1 Peripherals configuration

For the needs of the project like PWM generation, ADC conversion, sensor capture, and communication the following peripherals are used:

- **SysTick** - system timer for RTOS,
- **TIM3, TIM4, TIM5** - internal timing purposes,
- **TIM17** - time base for HAL library,
- **HRTIM1** - high resolution PWM generation,
- **TIM1** - XOR Input Capture for Hall sensor signal capture,
- **TIM2** - encoder signal capture,
- **ADC1, ADC2, ADC3, ADC4, ADC5** - back-EMF signal conversion and current sensing,
- **OPAMPs** - ADC signal conditioning,
- **FDCAN2** - communication with the main controller,

- **USB FS** - logging and DFU firmware update,
- **I2C2** - non-volatile EEPROM memory,
- **I2C1, SPI3** - external digital sensors.

5.3 PWM generation

To regulate voltage applied to the motor phases, a Pulse Width Modulation (PWM) signal is generated by the microcontroller. The microcontroller has a built-in HRTIM (High Resolution Timer) which has advantage over standard timers in terms of resolution and frequency, because its clock source can be higher than the `SYSCLK` thanks to integrated secondary PLL. According to HRTIM cookbook [24] the maximum counting frequency of the HRTIM is about 5.5GHz what with conjunction with 16-bit resolution provides very fine control of duty cycle while maintaining switching frequency above acoustic range (> 20kHz). The HRTIM contains 6 sub-timers which can be used independently or in synchronization and additional Master Timer which can be used to generate triggers for other peripherals. Each sub-timer controls two independent output pins. In this project, the HRTIM is used to generate 6 PWM signals for 6 power switches of the inverter. To generate signals 3 timers has been used with two output channels per half-bridge utilizing 2 separate compare registers. The `HIGH` state is generated when the counter is below the compare value and the `LOW` state is generated when the counter is above the compare value. According to datasheet `HRTIM` is not able to produce 100% duty cycle signal.

5.4 Hall sensor capture

To determine the rotor position for the needs of sensor-based control method, the Hall sensor signals are captured by the microcontroller via special timer mode called `XOR Input Capture`. According to TIM Cookbook [25] the XOR mode allows to capture the signal on both edges of multiple input channels and pass the event into the capture/compare unit. This process is depicted in Fig. 5.2. Each signal change generates an interrupt which is used to calculate the time between the rising and falling edges of the signal. The time between the edges is used to determine the rotor speed taking into account the number of pole pairs of the motor. Inside the interrupt routine, program reads state of the sensor pins and selects the next commutation state based on provided lookup table.

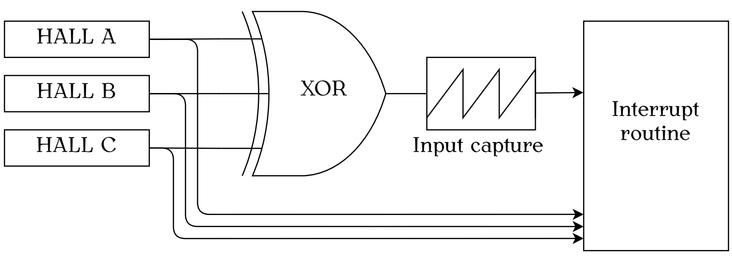

Figure 5.2 Diagram of Hall sensor capture diagram

5.5 Back-EMF capture

To determine the rotor position for the needs of sensorless control method the back-EMF signals are captured by the microcontroller via analog to digital converters (ADC). The back-EMF signals are generated by the motor windings and sensing the unpowered winding voltage allows to determine the rotor position. The measured signal differs when the other phases are in PWM `HIGH` state and when they are in `LOW` state and on edges of the PWM signal. Because of inductive nature of the motor, during turning off the PWM signals there is a voltage spike which can lead to misinterpretation of the signal. To avoid this problem, the ADC is triggered by the HRTIM intact with the PWM signal. Fig. 5.3 shows the PWM signal generation and ADC triggers. The Master Timer of the HRTIM has been configured utilize additional compare registers to generate triggers for the ADC. Compare value of ADC trigger is set to half of the PWM compare to align the ADC conversion with center of the PWM signal. To speed up the conversion multiple ADC units are used in parallel to measure all three back-EMF signals simultaneously. Utilized ADCs are used in Injected Conversion mode which has dedicated registers for storing the conversion results and generate interrupt when all conversions are done. The interrupt routine then stores the results in a window (circular buffer) which is reanalyzed with every new sample.

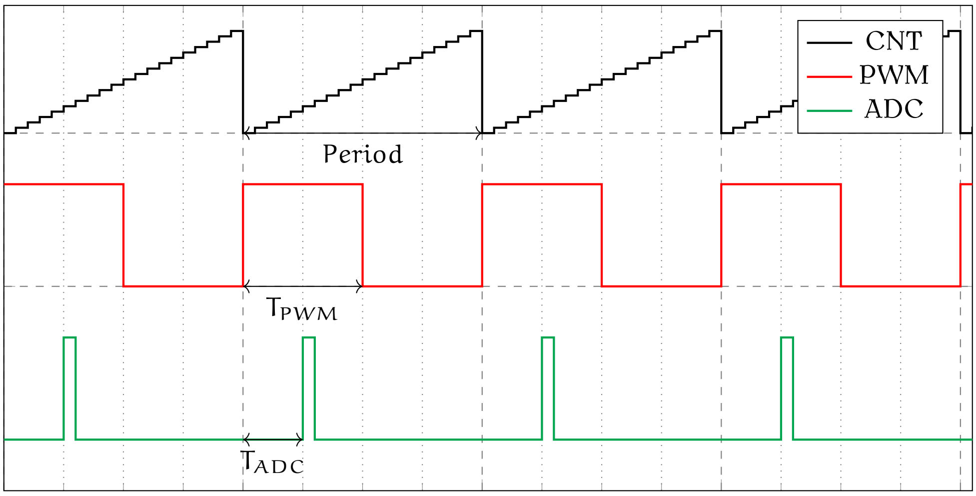

Figure 5.3 PWM generation and ADC triggering

5.6 System architecture

The software is divided into multiple tasks which are running concurrently. The tasks are scheduled by the FreeRTOS operating system running at 1000Hz preemption frequency. The system architecture is depicted in Fig. 5.4. Communication with the main controller (user) is done via CAN bus during runtime and USB during development. Device receives commands like start/stop or new speed set point via CAN bus in separate task which is responsible for parsing the received messages and pushing them into the queue. Command handler task reads the queued commands and updates the control variables. The control loop task periodically run the control algorithms and updates the PWM signals according to the calculated values in PI regulator. Statistics and debug information are sent to telemetry task which packs the data and sends it to the main controller via CAN bus transmission queue. Main commutation events are handled via interrupt routines to ensure proper timing and synchronization with the PWM signals.

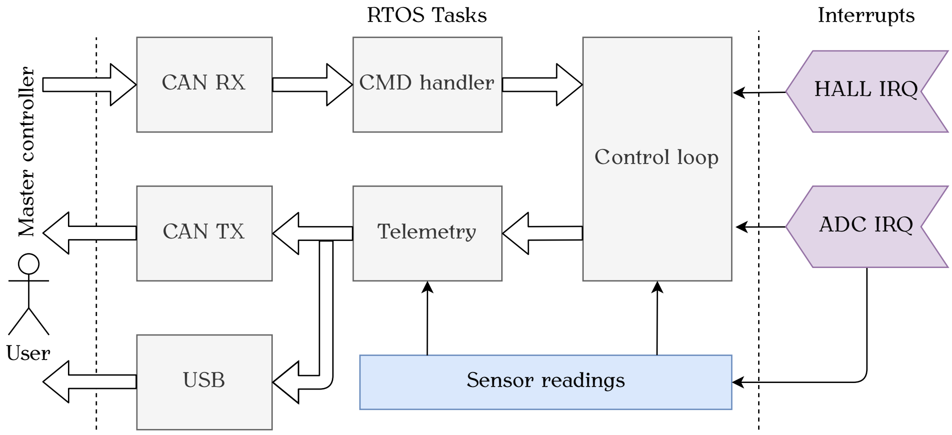

Figure 5.4 Diagram of tasks and data flow in the system

5.6.1 Startup procedure

Detailed diagram of the startup procedure is depicted in Fig. 5.5. The control loop is implemented as a Finite State Machine (FSM) with 3 states: `IDLE`, `START` and `RUN`. These states are automatically changed depending on current motor conditions and user commands. When controller receives a start command, it unlocks the motor and starts the control loop, but in `IDLE` state. When new speed set point is received and motor is not rotating, the state is changed to `START` and the start procedure corresponding to the selected control method is executed. When the motor is rotating, the state is changed to `RUN` and the speed regulation can be performed.

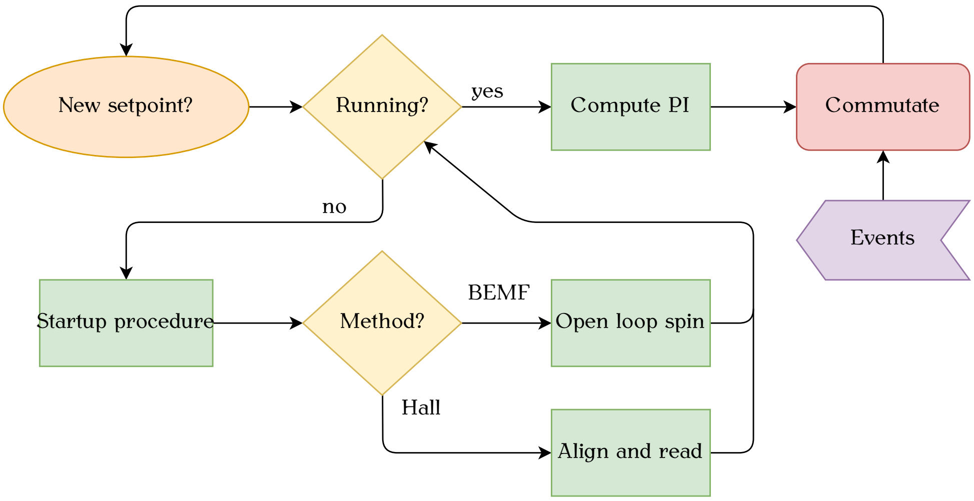

Figure 5.5 Diagram of startup procedure in the control loop

5.6.2 Commutation procedure

Detailed diagram of the commutation procedure for both sensor-based and sensorless control methods is depicted in Fig. 5.6. As previously described both Hall sensor and back-EMF signals acquisition are associated with interrupt routines. For sensor-based control method, this is the `Input Capture` interrupt of TIM1 timer. Each interrupt triggers the commutation procedure which reads the state of the Hall sensors and selects the next commutation state based on the lookup table. For sensorless control method, this is the `ADC Injected Conversion` interrupt. This time the interrupt only provides new sample which is stored in the window and analyzed in the with every new sample. Analogously to the sensor-based method, the commutation state is selected based on the lookup table after detecting the zero-crossing event in stored samples window. After selecting the commutation state, new timer is enabled to trigger another interrupt which will update the PWM signals to selected commutation state.

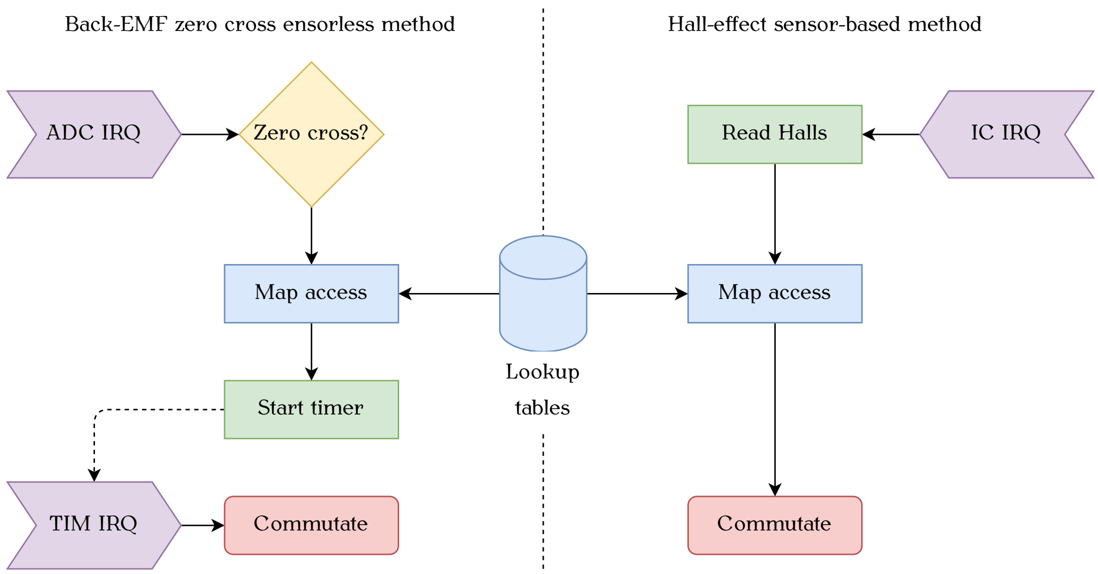

Figure 5.6 Diagram of commutation procedure for both methods

Chapter 6

Comparison of selected control methods

This chapter presents a study of sensor-based and sensorless methods for controlling brushless direct current (BLDC) motors, focusing on comparing the six-step commutation method using Hall sensors with the sensorless commutation method based on back electromotive force (BEMF) zero crossing detection.

6.1 Experimentation methodology

For purpose of the research a measurement station has been prepared. It consists of following components:

- 1kW inrunner BLDC motor with 9 slots and 6 poles,
- 2.7kW outrunner BLDC motor with 12 slots and 14 poles,
- 12V laboratory power supply,
- custom electronic speed controller (ESC),
- computer connected to the ESC via USB and CAN,
- 4 channel digital oscilloscope Siglent SDS1104X-E,
- optical tachometer DT-2234C.

Firstly, the operation of selected control methods was evaluated in open-loop mode. The motor was supplied with a constant voltage and the commutation signals were generated by the ESC. The oscilloscope was used to measure the phase voltages. After that, the motor was tested in closed-loop mode. The optical tachometer was used to measure the rotor speed. The ESC was controlled by the computer, which allowed to change the control method and the motor speed. It was done by sending CAN messages via simple python script.

6.2 Sensored control method evaluation

As described in chapter 3.2.1, the sensored control method uses Hall-effect sensors to detect the rotor position. The start sequence for this method relies on energizing the motor to first step position and measuring the hall sensors electrical state. After the first interrupt after aligning the rotor, the motor starts running in the six-step commutation mode.

6.2.1 First experiment

For conducing first experiment, the 1kW inrunner BLDC motor was used. The motor was connected to the ESC and the ESC was powered by the laboratory power supply. Then the sensor-based control method was selected and the motor was started. Fig. 6.1 shows the scope capture of the motor phases and one of the Hall sensors.

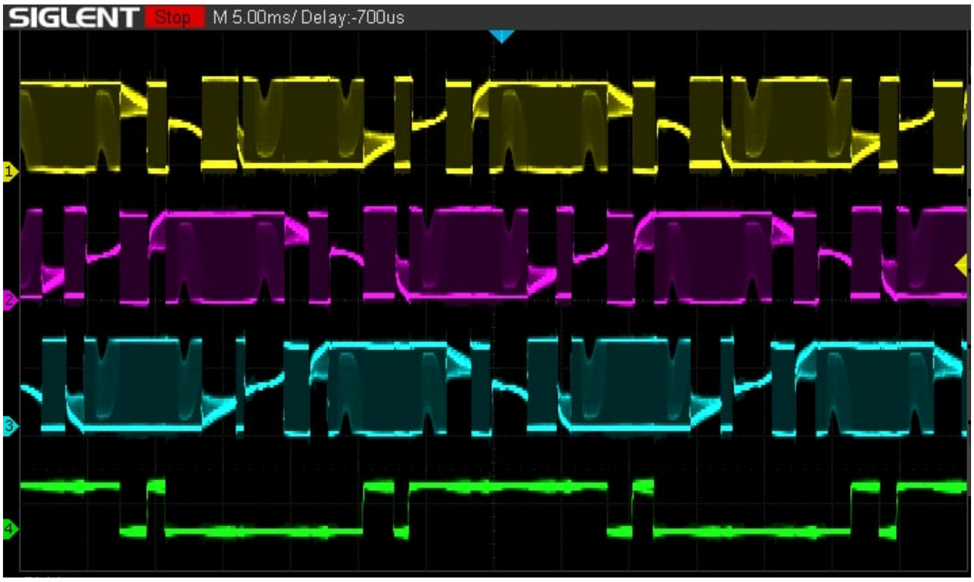

Figure 6.1 Scope capture of motor phases and one of the Hall sensors

We can clearly observe that although the motor is running, the Hall sensor signal is not stable and the motor is commutated incorrectly. This can be caused by the wrong Hall sensor placement or some electrical issue in the sensor itself. As mentioned in chapter 3.2 the research [3] shows that the high precision of the Hall sensor placement is crucial for stability of motor operation. Beside of the sensor signal unstability, detailed analysis of back electromotive forces (BEMF) shows that some of detected edges are actually false positives, but others are correct. Back electromotive forces generated on unpowered phases are diverging to voltage levels forced by the ESC and are symmetrical.

Hall sensor instability could be overcome by using some kind of filtration, but due to pulse width dependence on motor speed, it would involve additional complexity in estimating the filtration range and would introduce delay in commutation what would affect the motor performance.

6.2.2 Second experiment

Second experiment was conducted using the 2.7kW outrunner BLDC motor. The motor was connected to the ESC and the ESC was powered by the laboratory power supply. Then the sensor-based control method was selected and the motor was started. Fig. 6.2 shows the scope capture of the motor phase voltages during RUN state for both counterclockwise and clockwise rotation. Fig. 6.3 shows the scope capture of the Hall sensors signals for both counterclockwise and clockwise rotation. These Hall sensors emit a LOW signal when the magnetic field is detected.

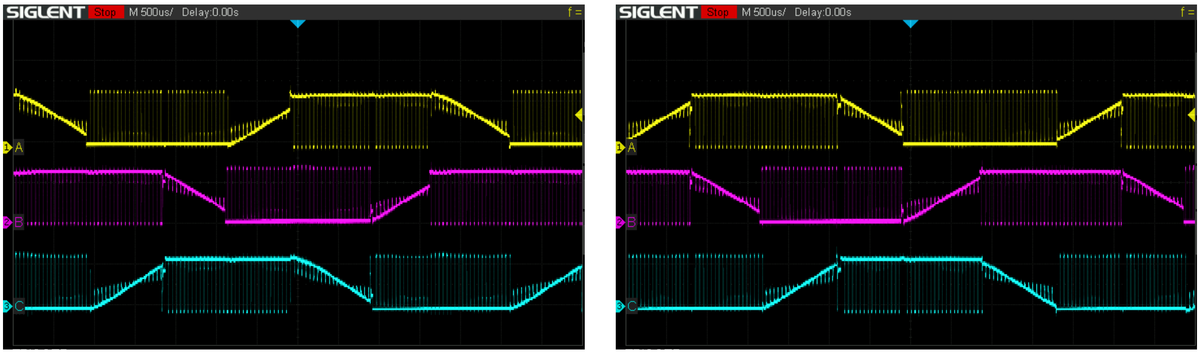

(a) Counterclockwise rotation (b) Clockwise rotation

Figure 6.2 Scope capture of the motor phase voltages

(a) Counterclockwise rotation (b) Clockwise rotation

Figure 6.3 Scope capture of the Hall sensors signals

We can observe that the phase voltages create 3 shifted by 120 degrees, trapezoidal waveforms. Because the motor is driven by the PWM signal, the voltage is not constant and there are visible ripples from the HIGH to LOW state, which is compliant with PWM duty cycle about 99%. Although the motor is running smoothly and commutation points seem to be correct, the phase voltages are not perfect trapezoidal waveforms. Commutation occurs when the back electromotive has not yet diverged to the voltage level forced by the ESC. This indicates that the motor is commutated too early, which can be caused again by the Hall sensor misplacement.

6.3 Sensorless control method evaluation

As described in chapter 3.3.1, the sensorless control method uses back electromotive force (BEMF) zero crossing detection to determine the rotor position. Fig. 6.4 shows the scope capture of the motor phase voltages during RUN state for counterclockwise rotation at 50% pulse width modulation (PWM) duty cycle. Fig. 6.5 shows the back electromotive forces measured by the ESC with marked commutation events.

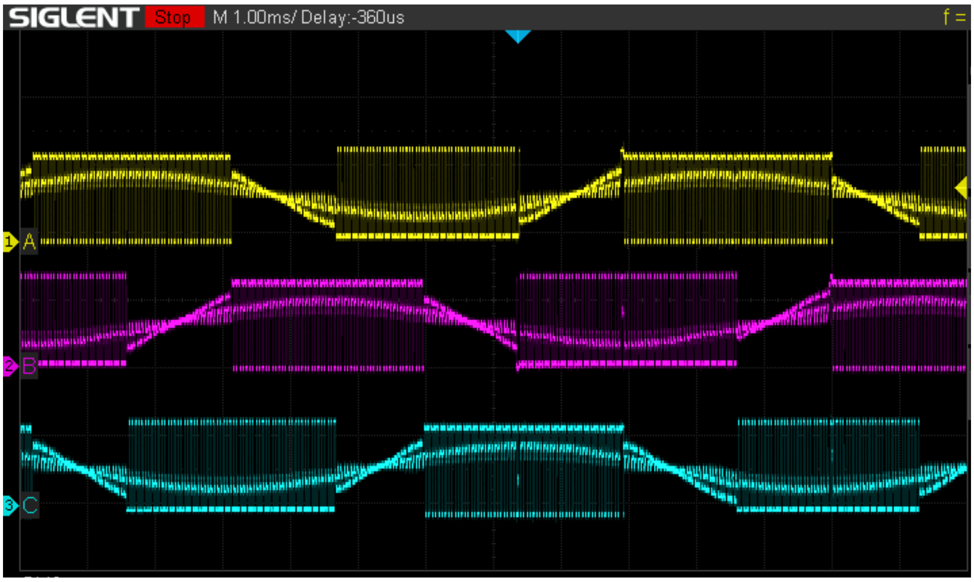

Figure 6.4 Scope capture of the motor phase voltages

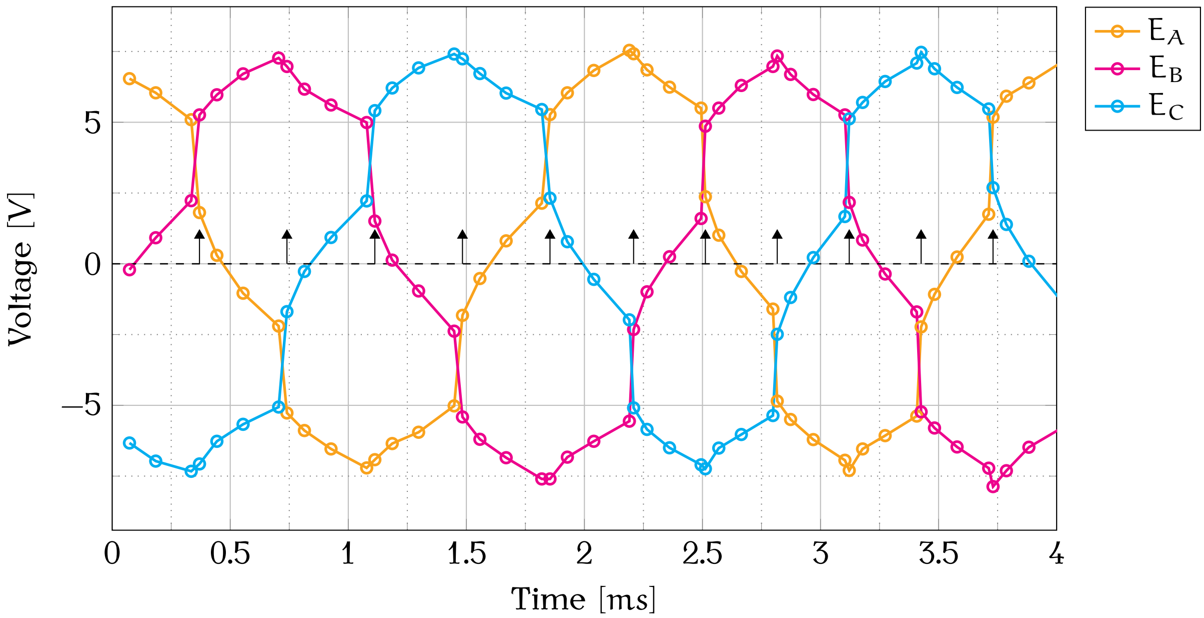

Figure 6.5 Phase back electromotive forces measured by the ESC and commutation events

The start sequence for this method relies on energizing the motor to first step position, then commutating the motor blindly with fixed time intervals and measuring the BEMF signals. After electromotive force is reasonably high, the motor starts commutating by counting time from zero crossing event.

We can observe that the phase voltages create 3 shifted by 120 degrees, trapezoidal waveforms. In contrast to the sensored control method, the back electromotive forces on unpowered phases are symmetrical and on both positive and negative voltage levels equally diverge into levels forced by the ESC.

The BEMF signals are symmetrical and have similar shape. Due to bandwidth limitations in real-time data transmission over CAN, the BEMF signals are decimated and have lower resolution than actual captured signals.

Despite from the above observations, discussed implementation of the sensorless control method has some limitations. For duty cycles below 50%, the BEMF signal is too weak to be properly detected. This leads to motor stalling and requires increasing the PWM duty cycle to start the motor. There were also complications with the BEMF zero crossing detection, which was not always accurate and sometimes led to motor stalling. This could be caused by noise in analog paths on the board.

Chapter 7

Conclusions

The aim of this thesis was to compare sensor-based and sensorless methods for controlling brushless direct current (BLDC) motors, focusing on the six-step commutation method using Hall sensors and the sensorless commutation method based on back electromotive force (BEMF) zero crossing detection.

Firstly, the theoretical review of BLDC motors fundamentals and the principles of sensored and sensorless control methods were presented.

For purpose of these methods comparison, a custom electronic speed controller (ESC) was designed, manufactured and assembly. Tests revelaed that the developed ESC provides solid foundation for experimentation on controlling BLDC motors with both sensored and sensorless methods.

The experimental analysis compared the two methods under various conditions, evaluating performance metrics such as efficiency, rotor position accuracy, and system reliability. Evaluation of these methods confirmed that they were both capable of controlling BLDC motors, but each had its own advantages and disadvantages.

Central thesis of this work was that the sensor based control method is more reliable than the sensorless method. The sensorless method was supposed to be more cost-effective, but less reliable especially at low speeds.

The results of the research confirmed that the sensor-based control method is more reliable at larger speed range and needs less time to start the motor. However, not every motor is equipped with Hall sensors, so it creates additional costs. What is more, the precise placement of the sensors is crucial for the stability of motor operation and rotor position estimation accuracy.

On the other hand, the sensorless method is more cost-effective and does not require additional sensors, but implementation of this method is more complex as it involves signal processing and precise time measurement. The sensorless method is also not suitable at low speeds, because the back electromotive force (BEMF) signal is too weak to be properly detected. Furthermore, the sensorless method is more prone to errors and requires more time to start the motor. However, from perspective of rotor synchronization accuracy, the sensorless method is better than the sensor-based method, because it does not rely on discrete Hall sensor signals, but uses continuous BEMF signal. It leads to smoother motor operation and better efficiency.

Therefore, the thesis has been confirmed, as the sensor-based method is more reliable at various speeds, but the sensorless method is more cost-effective and provides better rotor synchronization accuracy. An additional conclusion is the significance of hall sensor placement, which is makes the sensor-based method less applicable in high efficiency applications.

As for the choice of the control method, it depends on the specific application requirements. For example sensor-based method is more suitable for low speed applications, where the motor needs to start quickly and operate reliably like in electric vehicles. On the other hand, sensorless method is more suitable for high speed applications, where the motor needs to operate efficiently and precisely like in drones or industrial fans.

The research presented in this thesis could be extended in several ways. The sensorless method could be improved by using more advanced signal processing algorithms, such as Kalman filter or phase locked loop (PLL). These algorithms could improve the accuracy of rotor position estimation and immunize the system against noise and disturbances.

The sensor-based method could be enhanced by using other types of sensors, such as encoders or resolvers. These sensors provide more accurate information about the rotor position and speed, which could improve the performance of the motor control system.

Finally, for applications where precise position control is required, a Field Oriented Control (FOC) method could be implemented. This method allows to control the motor in a more efficient way. FOC method is more complex than the six-step commutation method, but it maximizes the torque output and minimizes the losses in the motor.

Bibliography

[1] B. Drudy and A. Hughes. *Electric Motors and Drives - Fundamentals, Types and Applications*. 5th ed. Newnes, 2019. ISBN: 978-00-8102-61-51.

[2] K. Krykowski. *Silniki PM BLDC - własności, sterowanie, aplikacje [BLDC PM Motors - properties, control, applications]*. 1st ed. BTC, 2015. ISBN: 978-83-64702-02-0.

[3] N. Samoylenko, Q. Han, and J. Jatskevich. "Dynamic Performance of Brushless DC Motors With Unbalanced Hall Sensors". In: *IEEE Transactions on Energy Conversion* 23.3 (2008), pp. 752–763. DOI: 10.1109/TEC.2008.921555.

[4] V. Aishwarya and B. Jayanand. "Estimation and control of sensorless brushless DC motor drive using Extended Kalman Filter". In: *2016 International Conference on Circuit, Power and Computing Technologies (ICCPCT)*. 2016, pp. 1–7. DOI: 10.1109/ICCPCT.2016.7530343.

[5] Y. Shao et al. "Sliding mode speed control for brushless DC motor based on sliding mode torque observer". In: *2015 IEEE International Conference on Information and Automation*. 2015, pp. 2466–2470. DOI: 10.1109/ICInfA.2015.7279700.

[6] Y. Wu, H. Zhao, and N. Zhao. "PLL control system based on FPGA for brushless DC motor". In: *Proceedings of the 33rd Chinese Control Conference*. 2014, pp. 7897–7902. DOI: 10.1109/ChiCC.2014.6896319.

[7] J. Shen and S. Iwasaki. "Sensorless control of ultrahigh-speed PM brushless motor using PLL and third harmonic back EMF". In: *IEEE Transactions on Industrial Electronics* 53.2 (2006), pp. 421–428. DOI: 10.1109/TIE.2006.870664.

[8] *LM5161 Wide Input 100-V, 1-A Synchronous Buck/Fly-Buck Converter*. Datasheet SNVSAE3B. Texas Instruments. 2016. URL: https://www.ti.com/lit/ds/symlink/lm5161.pdf.

[9] *TPS543x 3A, Wide Input Range, Step-Down Converter*. Datasheet SLV632K. Texas Instruments. 2006. URL: https://www.ti.com/lit/ds/symlink/tps5430.pdf.

[10] *AMS1117 1A Low Dropout Voltage Regulator*. Datasheet. Advanced Monolithic Systems. URL: https://www.advanced-monolithic.com/pdf/ds1117.pdf.

[11] *DRV835x 100-V Three-Phase Smart Gate Driver*. Datasheet SLVSDY6A. Rev. A. Texas Instruments. 2018. URL: https://www.ti.com/lit/gpn/drv8353.

[12] *IPT015N10N5 OptiMOS5 Power-Transistor*. Datasheet. Rev. 2.4. Infineon. 2023. URL: https://www.infineon.com/dgdl/Infineon-IPT015N10N5-DataSheet-v02_04-EN.pdf?fileId=5546d4624a75e5f1014ac94680661aff.

[13] *IR2108 Half-Bridge Gate Driver*. Data Sheet No. PD60161-R. International Rectifier. URL: https://www.farnell.com/datasheets/98473.pdf.

[14] *ACS72981xLR High-Precision Linear Hall-Effect-Based Current Sensor IC*. Datasheet. Allegro MicroSystems. 2024. URL: https://www.allegromicro.com/-/media/files/datasheets/acs72981-datasheet.pdf.

[15] *INA149 High Common-Mode Voltage Difference Amplifier*. Datasheet SBOS579B. Texas Instruments. 2011. URL: https://www.ti.com/lit/ds/symlink/ina149.pdf.

[16] *ESD protection of STM32 MCUs and MPUs application note*. Application note AN5612. Rev. 1. STMicroelectronics. 2022. URL: https://www.st.com/resource/en/application_note/an4776-generalpurpose-timer-cookbook-for-stm32-microcontrollers-stmicroelectronics.pdf.

[17] *SN65HVD23x 3.3-V CAN Bus Transceivers*. Datasheet SLOS346O. Texas Instruments. 2001. URL: https://www.ti.com/lit/ds/symlink/sn65hvd230.pdf.

[18] *STM32G474xC Arm Cortex-M4 32-bit MCU*. Datasheet DS12288. Rev. 6. STMicroelectronics. 2021. URL: https://www.st.com/resource/en/datasheet/stm32g474cb.pdf.

[19] *STM32G4 series advanced Arm-based 32-bit MCUs*. Reference manual RM0440. Rev. 8. STMicroelectronics. 2024. URL: https://www.st.com/resource/en/reference_manual/rm0440-stm32g4-series-advanced-armbased-32bit-mcus-stmicroelectronics.pdf.

[20] *STM32 Cortex-M4 MCUs and MPUs*. Programming manual PM0214. Rev. 10. STMicroelectronics. 2020. URL: https://www.st.com/resource/en/datasheet/stm32g474cb.pdf.

[21] R. Barry. *FreeRTOS reference manual: API functions and configuration options*. Real Time Engineers Limited, 2009.

[22] J. Wellbelove. *Embedded Template Library*. URL: https://www.etlcpp.com/.

[23] STM32CubeMX. *Microcontroller initialization code generator*. URL: https://www.st.com/en/development-tools/stm32cubemx.html.

[24] *HRTIM cookbook*. Reference manual AN4539. Rev. 4. STMicroelectronics. 2020. URL: https://www.st.com/resource/en/application_note/an4539-hrtim-cookbook-stmicroelectronics.pdf.

[25] *General-purpose timer cookbook for STM32 microcontrollers*. Application note AN4776. Rev. 3. STMicroelectronics. 2019. URL: https://www.st.com/resource/en/application_note/an4776-generalpurpose-timer-cookbook-for-stm32-microcontrollers-stmicroelectronics.pdf.

[26] KiCad EDA. *Project website*. URL: https://www.kicad.org/.

List of Tables

List of Figures

Appendix A

Electronic Schematics

This appendix contains the electronic schematics of the designed electronic speed controller (ESC) for brushless direct current (BLDC) motors. The schematics are divided into two parts: the main ESC electronics and the assembly schematics. The main ESC electronics schematics detail the design of the power stage, micro-controller, and peripheral components. The assembly schematics provide a visual representation of the physical layout of the components on the printed circuit board (PCB). Schematics were created using the KiCad [26] open-source software suite. The board layout renders are also included for reference.

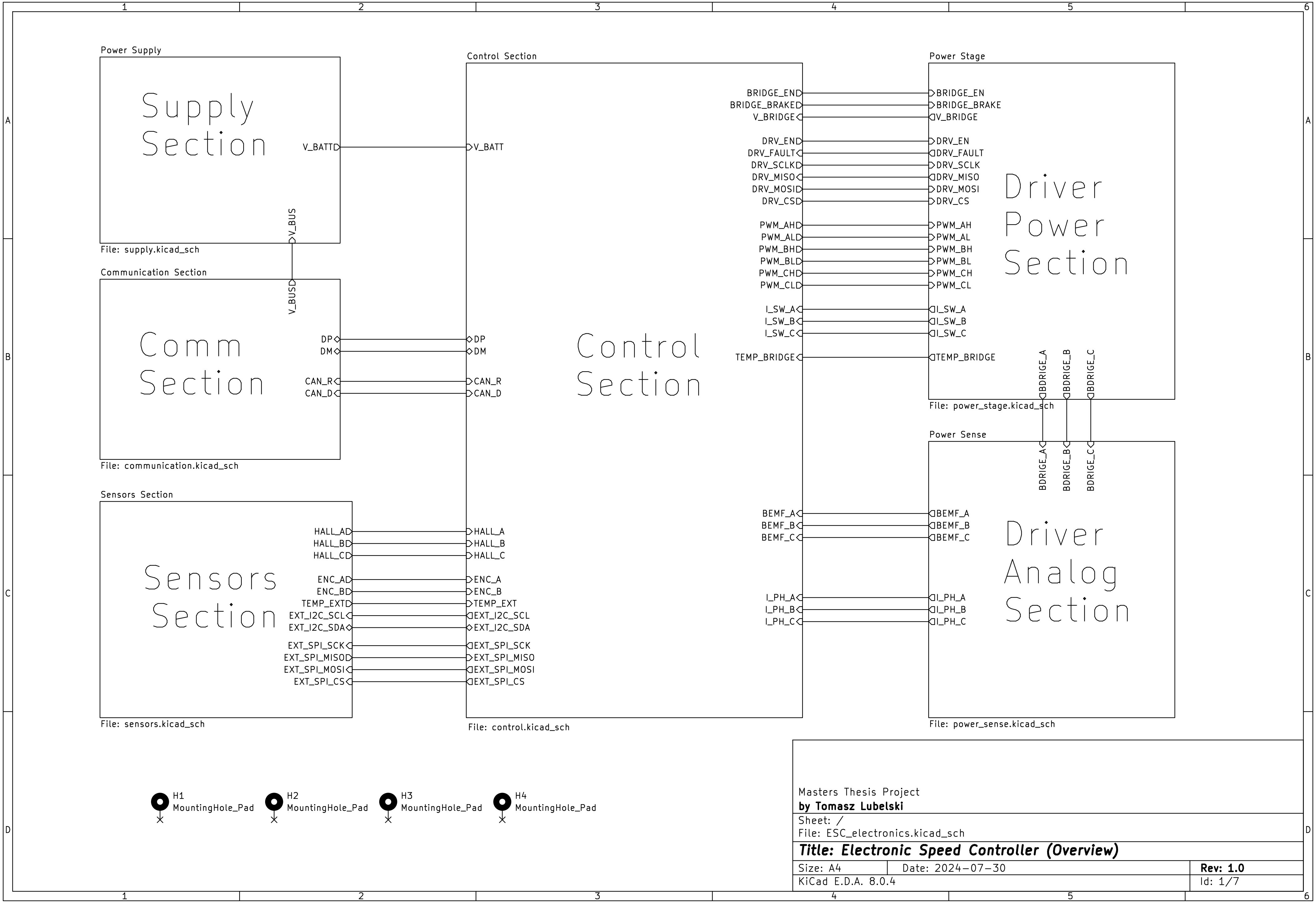
Power Supply
Supply Section
V_BATT
V_BUS
File: supply.kicad_sch
Communication Section
Comm Section
V_BUS
DP
DM
CAN_R
CAN_D
File: communication.kicad_sch
Sensors Section
Sensors Section
HALL_A
HALL_B
HALL_C
ENC_A
ENC_B
TEMP_EXT
EXT_I2C_SCL
EXT_I2C_SDA
EXT_SPI_SCK
EXT_SPI_MISO
EXT_SPI_MOSI
EXT_SPI_CS
File: sensors.kicad_sch
Control Section
Control Section
V_BATT
DP
DM
CAN_R
CAN_D
HALL_A
HALL_B
HALL_C
ENC_A
ENC_B
TEMP_EXT
EXT_I2C_SCL
EXT_I2C_SDA
EXT_SPI_SCK
EXT_SPI_MISO
EXT_SPI_MOSI
EXT_SPI_CS
BRIDGE_EN
BRIDGE_BRAKE
V_BRIDGE
DRV_EN
DRV_FAULT
DRV_SCLK
DRV_MISO
DRV_MOSI
DRV_CS
PWM_AH
PWM_AL
PWM_BH
PWM_BL
PWM_CH
PWM_CL
I_SW_A
I_SW_B
I_SW_C
TEMP_BRIDGE
BEMF_A
BEMF_B
BEMF_C
I_PH_A
I_PH_B
I_PH_C
File: control.kicad_sch
Power Stage
Driver Power Section
BRIDGE_EN
BRIDGE_BRAKE
V_BRIDGE
DRV_EN
DRV_FAULT
DRV_SCLK
DRV_MISO
DRV_MOSI
DRV_CS
PWM_AH
PWM_AL
PWM_BH
PWM_BL
PWM_CH
PWM_CL
I_SW_A
I_SW_B
I_SW_C
TEMP_BRIDGE
BDRIGE_A
BDRIGE_B
BDRIGE_C
File: power_stage.kicad_sch
Power Sense
Driver Analog Section
BDRIGE_A
BDRIGE_B
BDRIGE_C
BEMF_A
BEMF_B
BEMF_C
I_PH_A
I_PH_B
I_PH_C
File: power_sense.kicad_sch
H1 MountingHole_Pad
H2 MountingHole_Pad
H3 MountingHole_Pad
H4 MountingHole_Pad
Masters Thesis Project
by Tomasz Lubelski
Sheet: /
File: ESC_electronics.kicad_sch
Title: Electronic Speed Controller (Overview)
Size: A4
Date: 2024-07-30
Rev: 1.0
KiCad E.D.A. 8.0.4
Id: 1/7

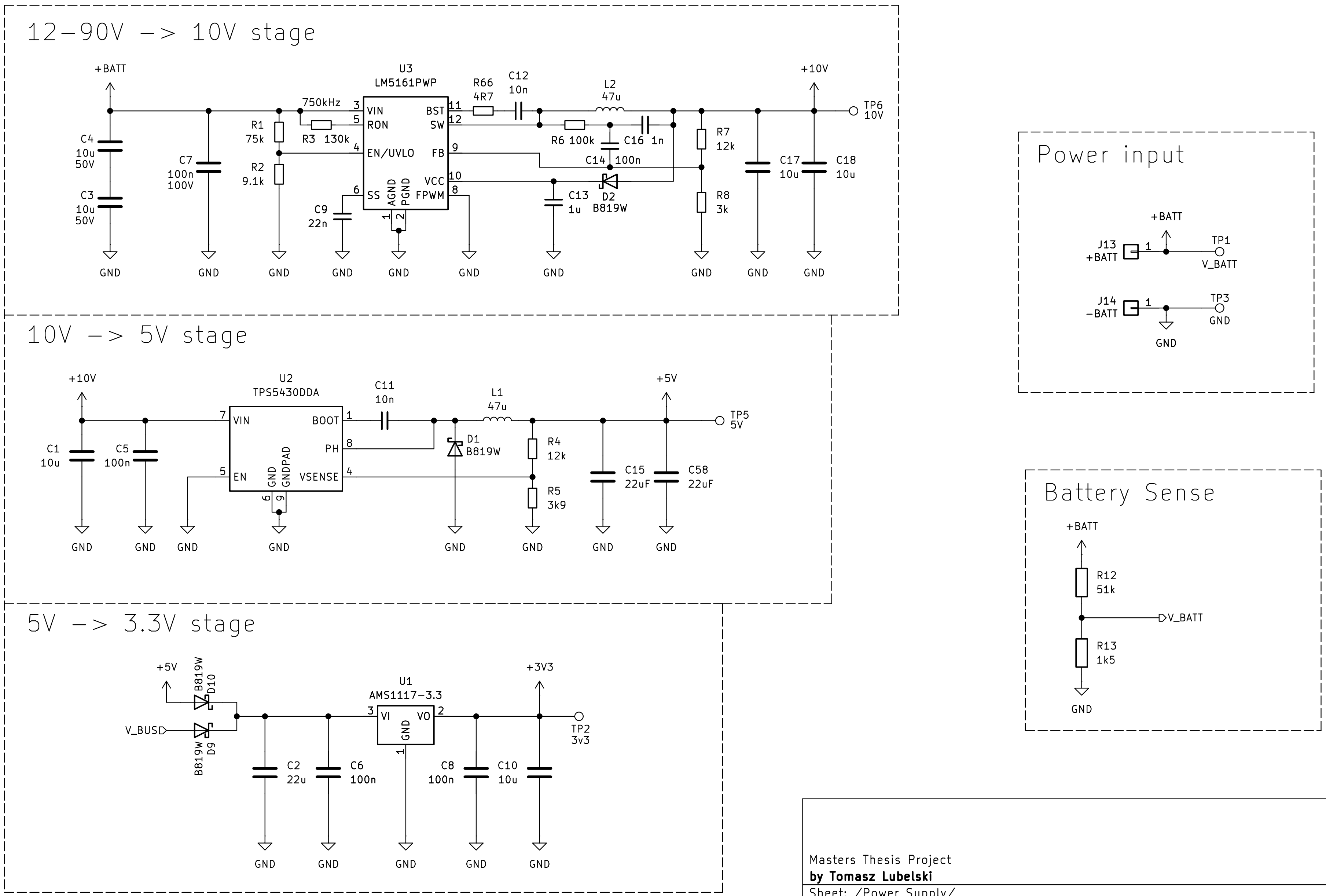

Masters Thesis Project
by Tomasz Lubelski

Sheet: /Power Supply/
File: supply.kicad_sch

Title: Electronic Speed Controller (Power supply)

Size: A4	Date: 2024-07-30	**Rev: 1.0**
KiCad E.D.A. 8.0.4		Id: 2/7

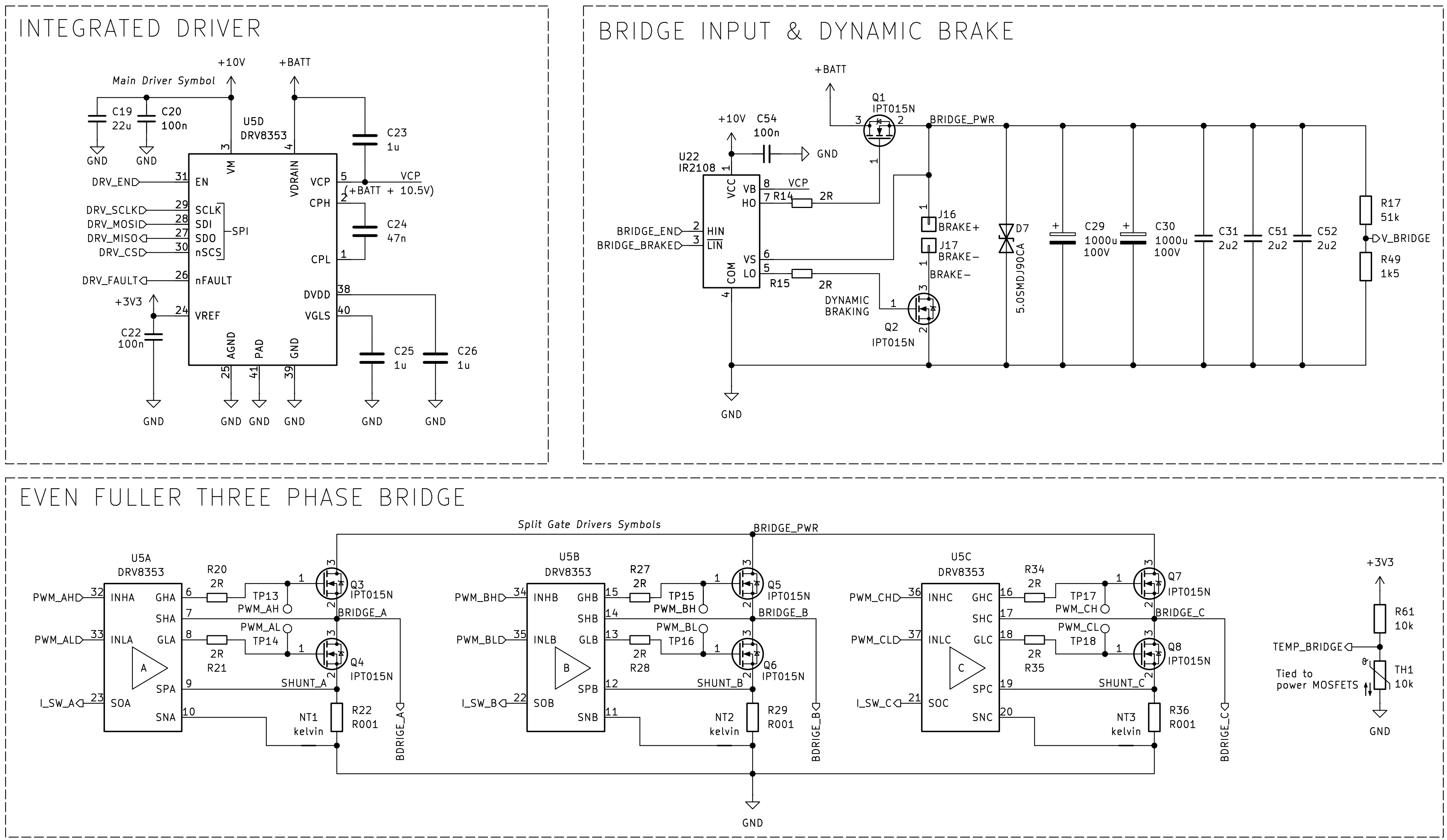

Masters Thesis Project
by Tomasz Lubelski

Sheet: /Power Stage/
File: power_stage.kicad_sch

Title: Electronic Speed Controller (Power Stage)

Size: A4	Date: 2024-07-30	**Rev: 1.0**
KiCad E.D.A. 8.0.4		Id: 3/7

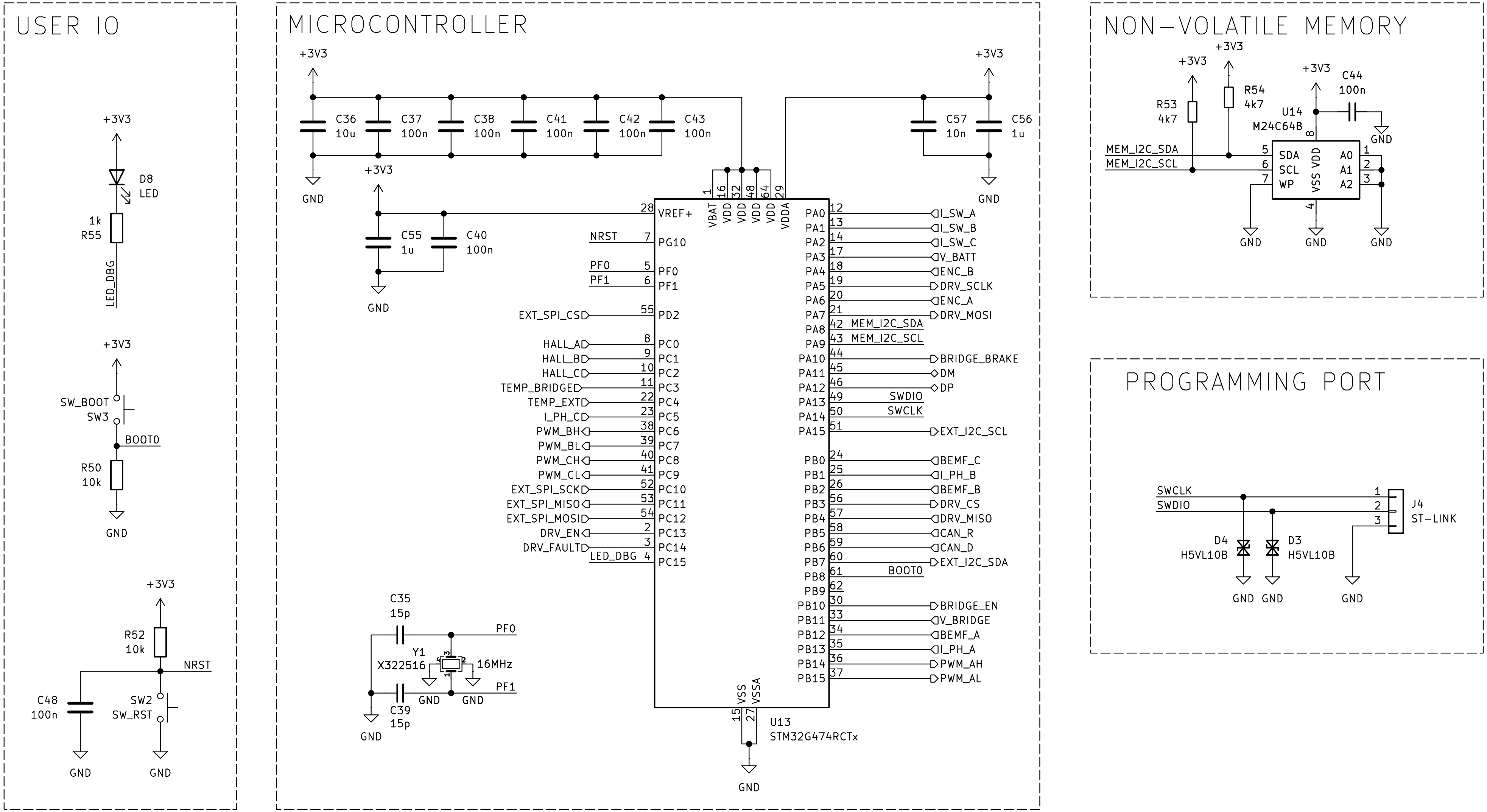

Masters Thesis Project
by Tomasz Lubelski

Sheet: /Control Section/
File: control.kicad_sch

Title: Electronic Speed Controller (Control section)

Size: A4 | Date: 2024−07−30 | **Rev: 1.0**
KiCad E.D.A. 8.0.4 | Id: 4/7

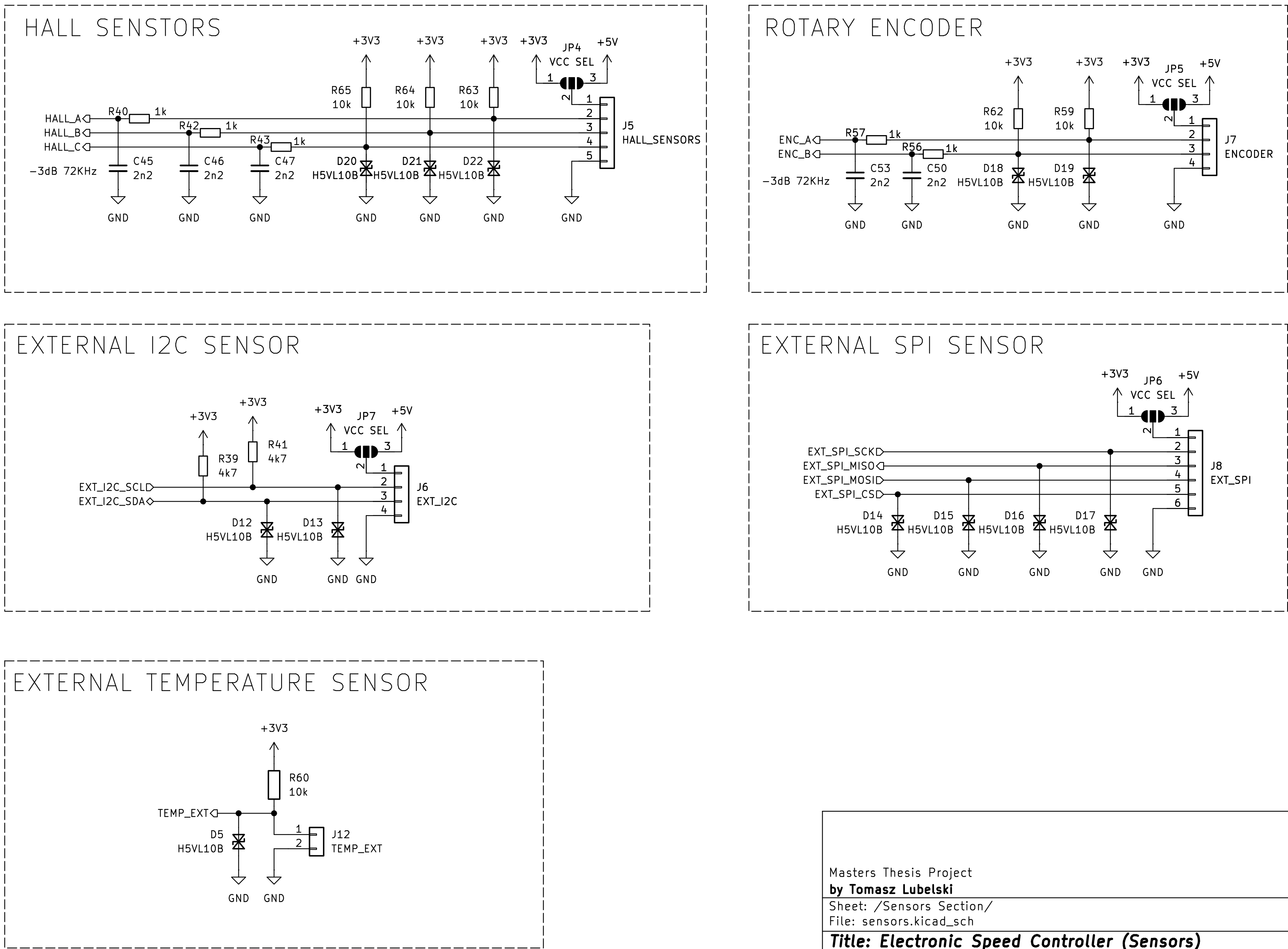

Masters Thesis Project
by Tomasz Lubelski

Sheet: /Sensors Section/
File: sensors.kicad_sch

Title: Electronic Speed Controller (Sensors)

Size: A4	Date: 2024-07-30	**Rev: 1.0**
KiCad E.D.A. 8.0.4		Id: 5/7

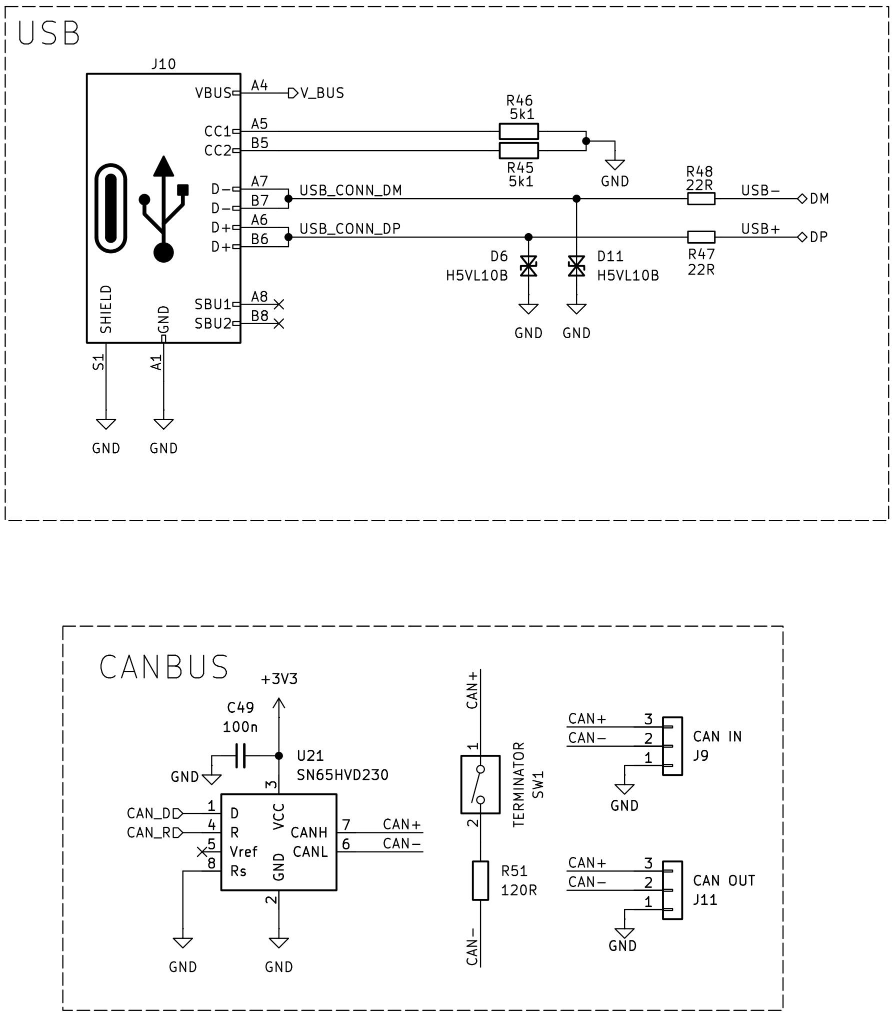

Masters Thesis Project
by Tomasz Lubelski

Sheet: /Communication Section/
File: communication.kicad_sch

Title: Electronic Speed Controller (Communication)

Size: A4	Date: 2024-07-30	**Rev: 1.0**
KiCad E.D.A. 8.0.4		Id: 6/7

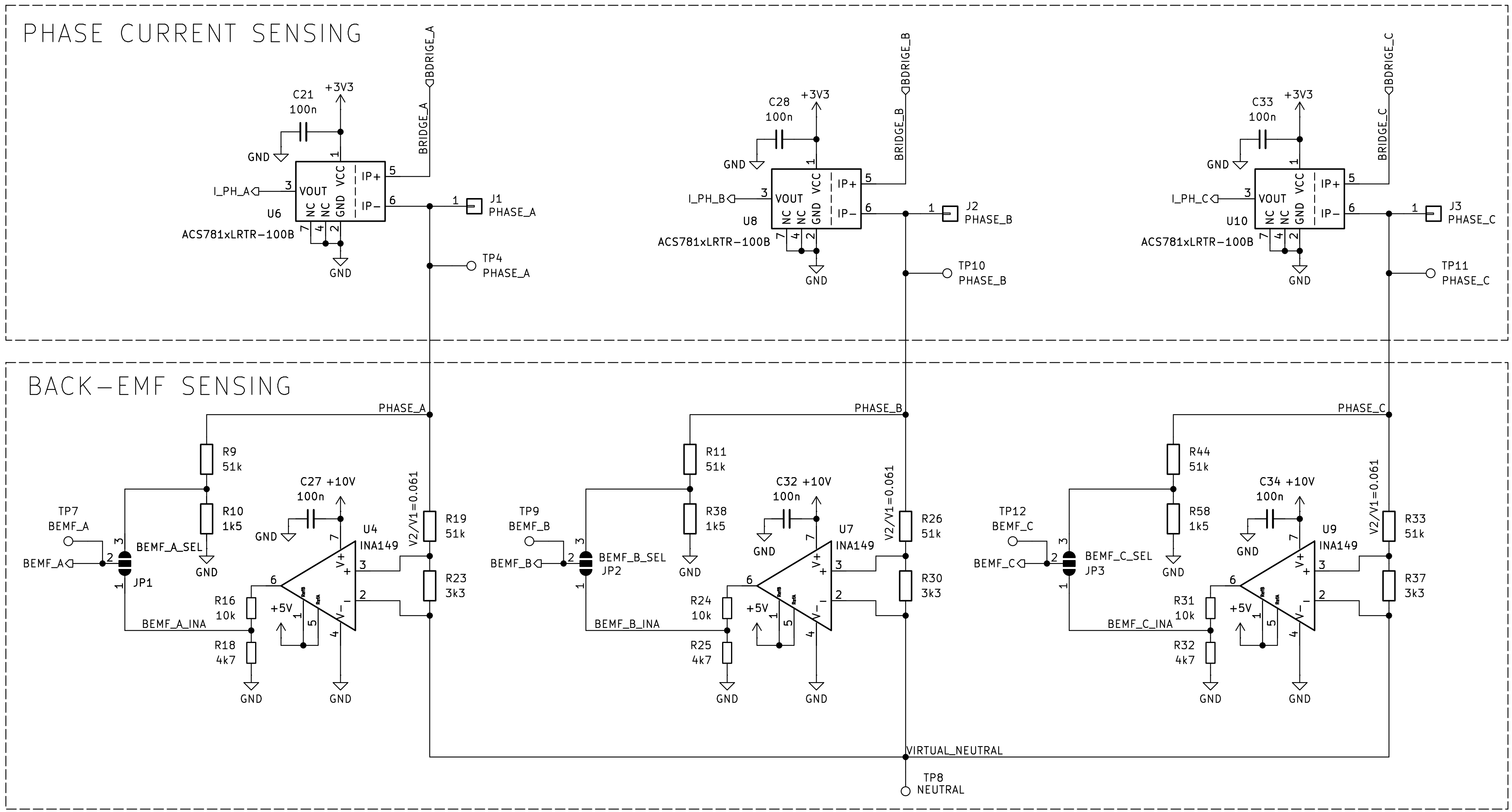

Masters Thesis Project

by Tomasz Lubelski

Sheet: /Power Sense/

File: power_sense.kicad_sch

Title: Electronic Speed Controller (Analog section)

Size: A4 | Date: 2024-07-30 | **Rev: 1.0**

KiCad E.D.A. 8.0.4 | Id: 7/7

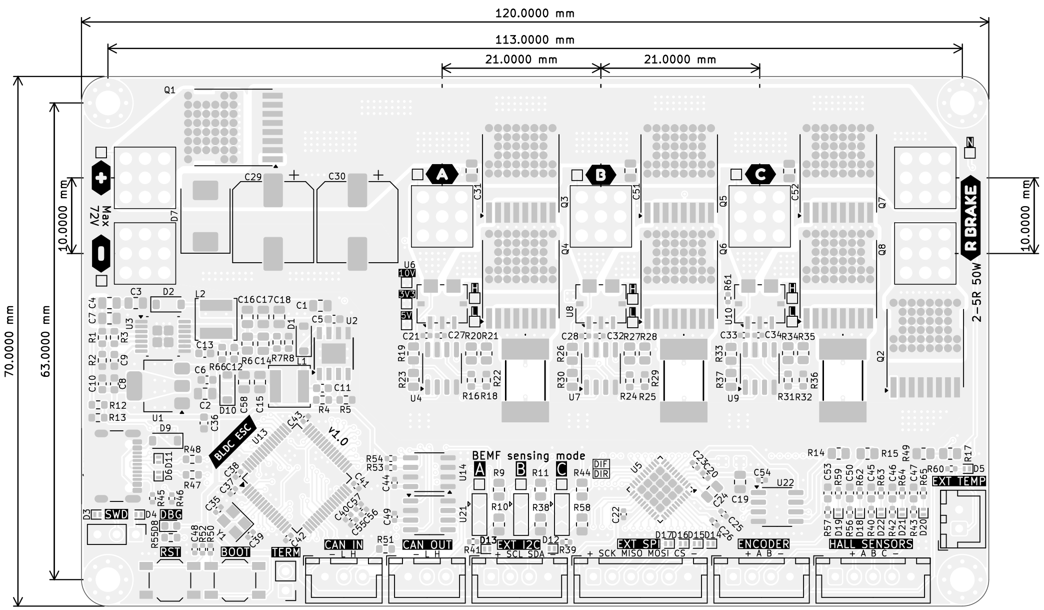

Masters Thesis Project **by Tomasz Lubelski**
Sheet: File: ESC_electronics.kicad_pcb
Title: Electronic Speed Controller
Size: A4 · Date: 2024-07-30 · **Rev:**
KiCad E.D.A. 8.0.4 · Id: 1/1

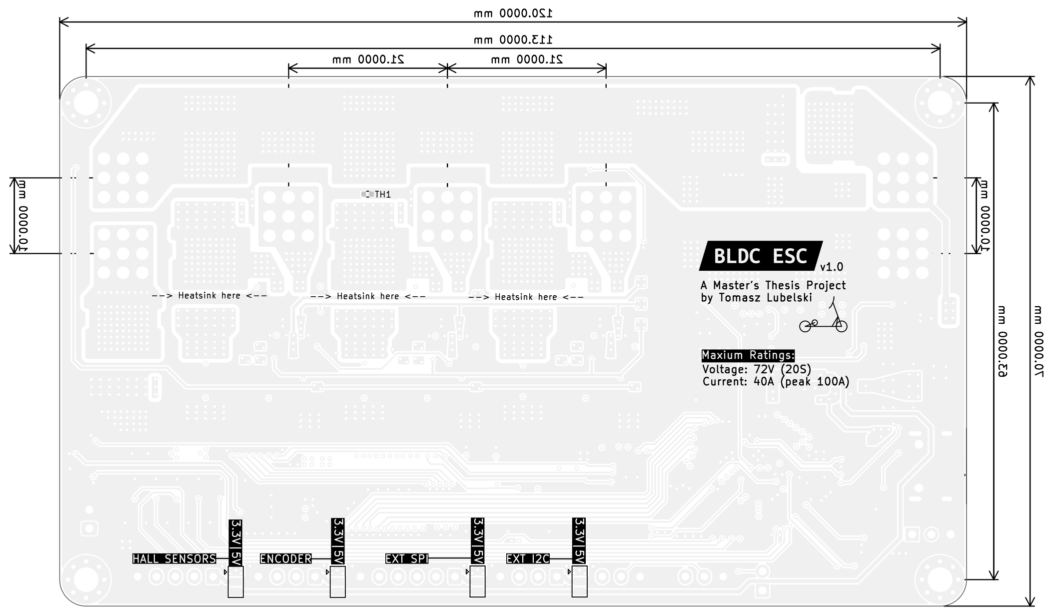

Masters Thesis Project **by Tomasz Lubelski**		
Sheet: File: ESC_electronics.kicad_pcb		
Title: Electronic Speed Controller		
Size: A4	Date: 2024-07-30	**Rev:**
KiCad E.D.A. 8.0.4		Id: 1/1

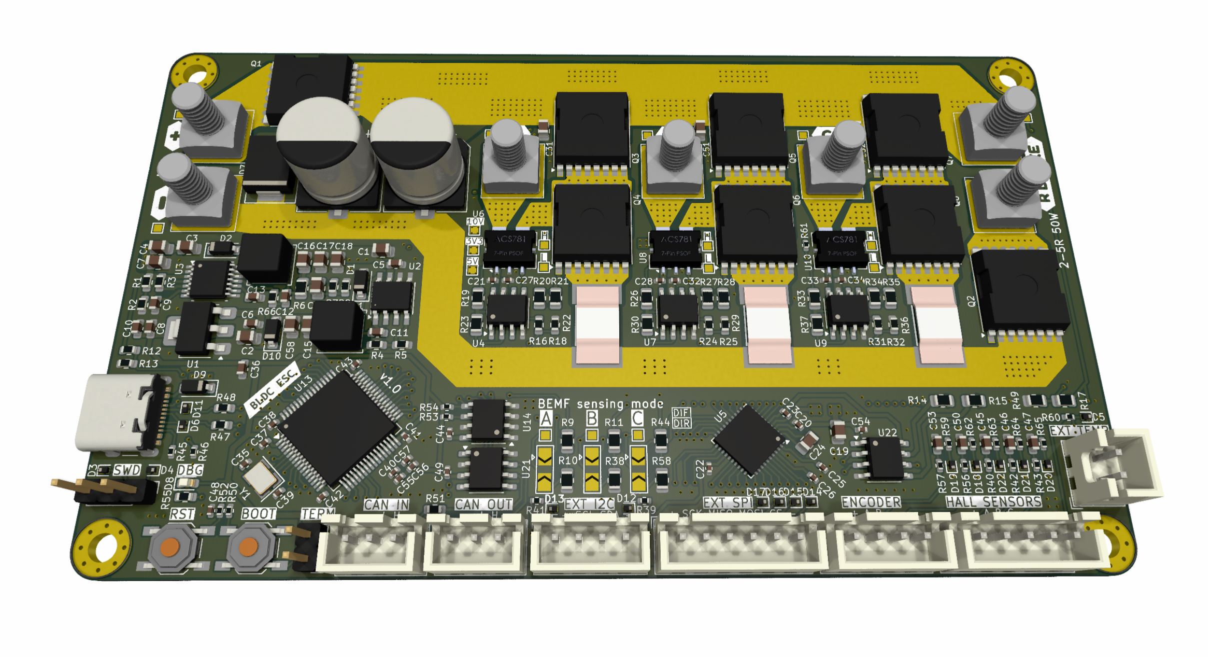

Figure A.1 Board layout render – top view.

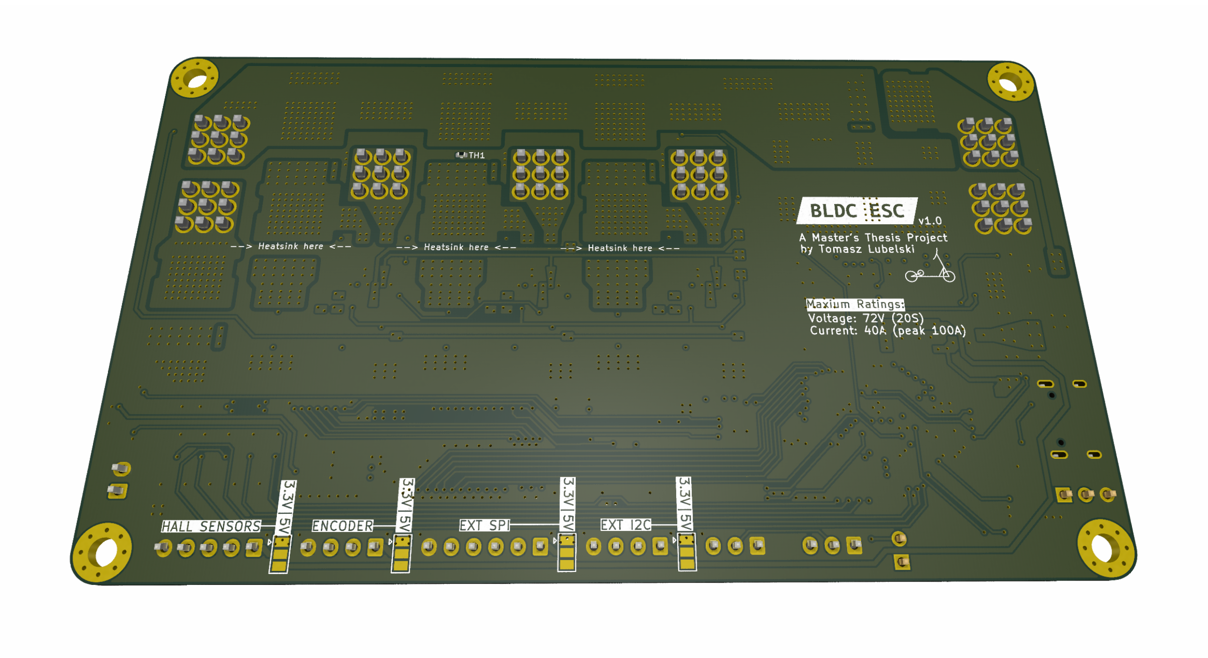

Figure A.2 Board layout render – bottom view.